DSA Report
Dec 2021, number 5

Environmental Impact Assessment of a hypothetical accident during ship transport of spent nuclear fuel from Andreeva Bay to FSUE ATOMFLOT

DSA
Norwegian Radiation
and Nuclear Safety Authority

Referanse

Brown JE, Hosseini A, Dowdall, M, Amundsen, I. Environmental Impact Assessment of Spent Nuclear Fuel transported from Andreeva Bay to FSUE ATOMFLOT.
DSA-rapport 2021:5. Østerås, Direktoratet for strålevern og atomsikkerhet, 2021.

Emneord

Andreeva Bay, Spent Nuclear Fuel, Transport, Environmental Impact Assessment

Resymé

Vurdering av potensielle miljøkonsekvenser av en ulykke under skipstransport av brukt atombrensel fra Andrejevbukta.

Reference

Brown JE, Hosseini A, Dowdall, M, Amundsen, I. Environmental Impact Assessment of Spent Nuclear Fuel transported from Andreeva Bay to FSUE ATOMFLOT.
DSA Report 2021:5. Østerås: Norwegian Radiation and Nuclear Safety Authority, 2021.
Language: Norwegian.

Key words

Andreeva Bay, Spent Nuclear Fuel, Transport

Abstract

Assessment of potential environmental consequences of an accident during transport of spent nuclear fuel by sea from Andreeva Bay.

Godkjent:

Ingar Amundsen, fung. avdelingsdirektør, avdeling kunnskapsutvikling og internasjonal atomsikkerhet

Publisert 2021-12-21
Sider 56

DSA,
Postboks 329,
0213 Oslo
Norge.

Telefon 67 16 25 00
Faks 67 14 74 07
Email dsa@dsa.no
dsa.no

ISSN 2535-7339

Environmental Impact Assessment of a hypothetical accident during ship transport of spent nuclear fuel from Andreeva Bay to FSUE ATOMFLOT

Contents

1 Background

The Andreeva Bay facility of the Northwestern Centre for Radioactive Waste Management 'SevRAO' and FSUE ATOMFLOT are both located on the Kola Peninsula. Andreeva Bay, located on the northwestern shore of the Kola Peninsula, lies some 45 km from the Russian-Norwegian border. FSUE ATOMFLOT is located in the Kola Bay on the northern periphery of Murmansk. Andreeva Bay was constructed and commissioned between 1961-1963 and functioned as a service base for nuclear submarines for some 25 years and also received, treated and stored (on a temporary basis) solid and liquid radioactive wastes (SRW and LRW). The facility stopped receiving spent nuclear fuel (SNF) and wastes in 1989. The current temporary SNF and RW storage facility at Andreeva Bay is managed by the Northwestern Centre for radioactive waste management SevRAO, branch of FSUE RosRAO (NWC SevRAO - branch of FSUE RosRAO). The facility is host to the SNF of approximately 100 nuclear submarine reactors and large amounts of radioactive waste, all stored under poor conditions. The Andreeva Bay site is being remediated and the most significant phase of the decommissioning is the removal of SNF from its current storage and its transport for processing.

The process of removal of SNF from the Andreeva Bay site, technical details regarding the SNF and its handling and the environmental implications of a possible release of activity during these operations have been previously assessed by Shilov et al. (2017) in a detailed assessment. This assessment included detailed information as to preventative and mitigatory systems and procedures put in place to minimize risk of and impact from accidental releases of radioactive materials. One aspect of the removal process that was not covered in great detail was the actual transport of the SNF by sea to FSUE ATOMFLOT. The passage to FSUE ATOMFLOT is a journey of approximately 100 km and takes 6 hours. The SNF is carried onboard the specially built, Italian funded nuclear fuel carrier *Rossita*, which has two isolated holds with a capacity of 720 tonnes. The SNF will be transported in transport casks of the designation TUK-108/1 and TK- 18 whith capacities of 49 spent fuel assemblies (SFA). TUK-108/1 (TUK-18) (type B (U) accord with relevant international standards for such containers and meet all requirements as outlined by the International Atomic Energy Agency (IAEA) as well as those outlined by relevant Russian regulatory bodies.

This report concerns itself with the potential environmental consequences of a release of activity during the transport of SNF by sea from Andreeva Bay to the facilities of FSUE ATOMFLOT, elements of which are funded by the Norwegian Governments Nuclear Action Plan.

2 Methodology

2.1 Source Term

For the estimation of a source term, reference was made to Shilov et al. (2017) which provides an impact assessment of various stages of the process for the removal of spent nuclear fuel from the Andreeva Bay facility. In the description of beyond design-based accidents, indicative figures are provided for the release fractions of ^{137}Cs and ^{90}Sr under various scenarios and the corresponding activity. Combination of the values facilitates a rough estimate of the activity of ^{137}Cs and ^{90}Sr contained within the 49 assemblies housed within 1 TUK container. Based on these values, the amount of ^{137}Cs and ^{90}Sr contained within 1 TUK was estimated as being 2.2×10^{14} Bq and 1.8×10^{14} Bq respectively.

For the purposes of simplicity and conservatism, consequences were estimated for the release of the entire contents one TUK cask. Adoption of these values has no bearing on estimating the probability of any particular accident type or release and served solely to facilitate estimation of consequences for a given amount of activity released. The amount should be considered as extremely conservative.

2.2 Scenario Description

For the purposes of the work reported upon here, hypothetical releases were considered as having occurred at each of three open water locations: the first at the mouth of Zapadnaya Litsa, the second midway between Andreeva Bay and Murmansk and the third at the mouth of the Kola Bay. It should be considered that all three are so close together that there is little or no difference oceanographically, from the perspective of the applied marine contaminant dispersion model, between the selected locations. Release points in the immediate vicinity of Andreeva Bay and FSUE ATOMFLOT were not chosen for two reasons; there were model limitations for near-shore release points and previous impact assessments have dealt with releases while loading and unloading at Andreeva Bay and FSUE ATOMFLOT respectively.

2.3 Modelling Methodology

2.3.1 Advection and dispersion of radionuclides in the marine environment

The circulation of the Barents Sea in the southwestern parts is characterized by a general motion of waters from west to east. Inflow from the Norwegian Sea takes place through the Bear Island Channel. Close to the coast, low salinity (S = 34.4) water of the Norwegian Coastal Current (NCC) carries runoff from the Baltic and the Norwegian coasts into the southern Barents Sea (Fig. 1, green, Fig. 2). It continues eastward as the Murmansk Coastal Current. Additional low salinity water is added as it passes the entrance to the White Sea and the mouth of the Pechora River, so the salinity remains low (S = 34.6). Most of this ‘‘coastal’’ water passes into the Kara Sea through the Kara Gate. River runoff and net precipitation are small, and the NCC is the major freshwater source for the Barents Sea (Tantsiura, 1959; Loeng, 1991). In addition, warm and salty Atlantic derived water of the Norwegian Atlantic Current in the Nordic Seas enters north of the coastal current and south of Bear Island (Fig. 1, red). On its way to the east, the warm water of Atlantic origin loses heat and several varieties of water densities are formed, part of these sink to the bottom of the Barents Seas. Approaching Novaya Zemlya, the Atlantic derived waters turn north while cooling down further. To the north, a strong front separates the Atlantic derived water masses from the cold and fresh waters stemming from the Arctic. These move southwestward and leave the Barents Sea between Svalbard and around Bear Island (Fig. 1, blue). The coastal currents are strongly density driven and thus a rather permanent feature (Fig. 2). This means that typically soluble substances releases

offshore of the coast of Murmansk will drift east, and northeast. However, in particular in summer months, the wind field patterns in the Barents Sea may induce westward motion also in the southern part for a few weeks (Harms and Karcher, 2005). Figure 3 shows a timeseries of typical surface (0-20m) velocities in the coastal current 50-100 km offshore from the Murrmansk coast as simulated by the NAOSIM model (see section III for a model description). The only extended period of westward flow in this area occurred in summer 1998, which was characterized by a specific weather pattern which suppressed the eastward flow and even led to westward return flow over larger areas in the southern Barents Sea and parts of the Kara Sea (e.g. Harms and Karcher, 2005). Further north, in the central Barents Sea and around the Central Bank (Fig. 1), currents are much more variable and easily can involve westward motion.

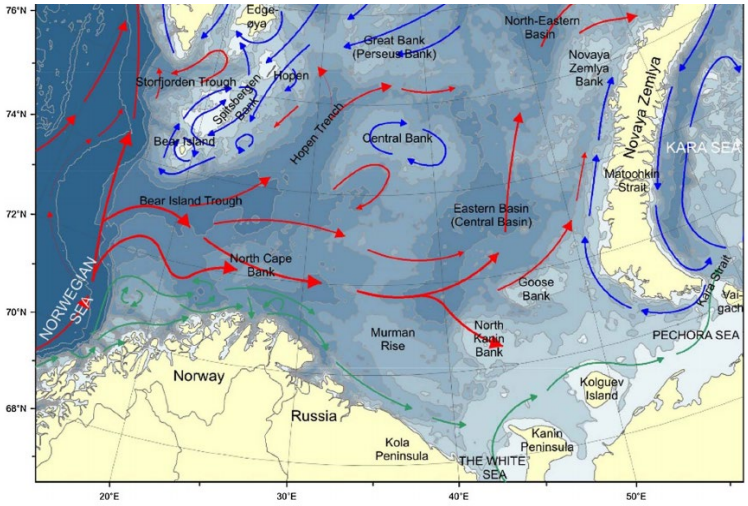

Figure 1: The Barents Sea. Red arrows show Atlantic water currents, blue arrows Arctic currents and green arrows currents of coastal waters (from Eriksen et al., 2017).

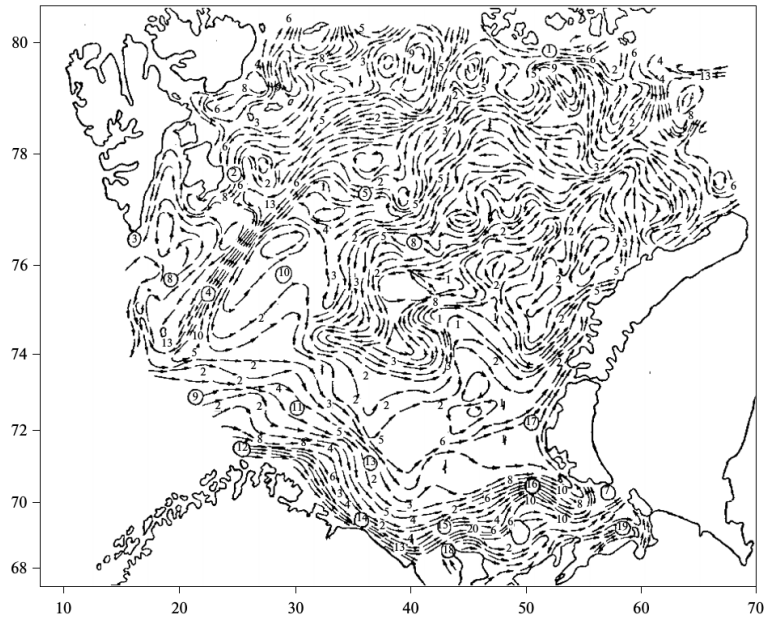

Figure 2: Spatial distribution of permanent surface density currents in the Barents Sea according to the results of diagnostic calculations (Terziev et al., 1990). Figures in circles are the serial numbers of currents. Figures without circles indicate velocity in cm/s (Kagan et al., 2015). Franz Josef Land Current (1), East Spitsbergen Current (2), Suidcap Current (3), Medvezhinskoe Current (4), Persey (Southwestern) Current (5), Central Current (6), Litke Current (7), warm permanent Southern Spitsbergen Current (8), Nordkap Current (9) (which is divided into the northern (10), central (11), and southern (12) branches), Murmansk Current (13), Murmansk coastal Current (14), Canin Current (15), Kolguev Pechora Current (16), Novaya Zemlya Current (17), discharge surface currents Belomorskoe (18) and Pechora (19).

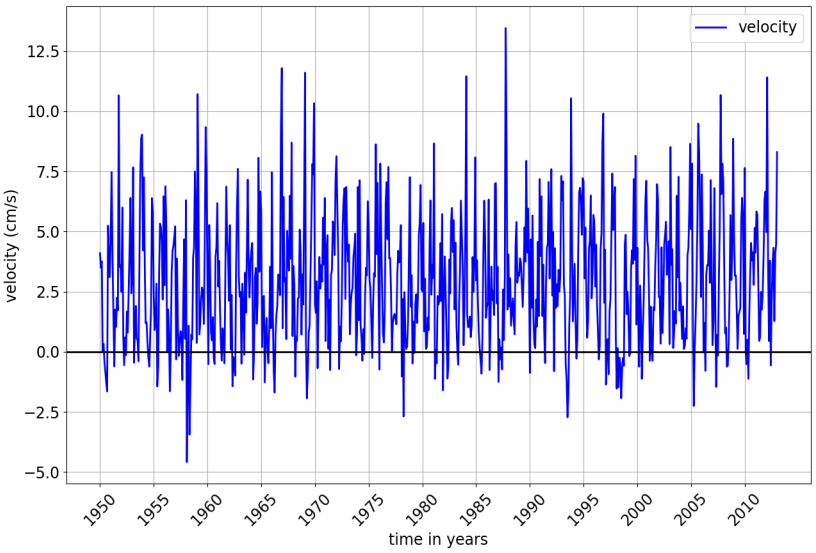

Figure 3: Simulated surface velocities (positive southeastward, along shore) (0-20m) about 60 km offshore of the coast near Murmansk, in the Murmansk coastal current (red dot in Fig. 2; NAOSIM, monthly means).

The numerical model used for the current set of experiments is a version of NAOSIM (North Atlantic/Arctic coupled Ocean Sea Ice Model) (Karcher et al., 2003; Köberle and Gerdes, 2003)). It is derived from the

Geophysical Fluid Dynamics Laboratory modular ocean model MOM-2 (Pacanowski, 1995) and incorporates a dynamic-thermodynamic sea ice model with a viscous-plastic rheology (Hibler, 1979). The version used here has 30 unevenly spaced levels in the vertical, starting from 20 m thickness down to 100 m depth with the thickness gradually increasing with depth. The model domain covers the Nordic Seas, the Arctic Ocean and the northern North Atlantic down to about 50ºN. The Canadian Archipelago allows throughflow between the central Arctic and the Labrador Sea. The model has an open boundary in Bering Strait where a total inflow for the barotropic mode of 0.8 Sv is imposed to cover approximate amount of observed inflow of Pacific Water into the Arctic Ocean. It also has an open boundary in the south, where barotropic flow from a larger scale version of the model is prescribed. At both boundaries the flow profiles can develop freely. The open boundary conditions have been implemented following Stevens (1991), thereby allowing the outflow of tracers and the radiation of waves. The initial hydrography in January 1948 is adopted from the PHC winter climatology (Steele et al., 2001), while a yearly mean climatology is used as a reference for surface salinity restoring on a time scale of 180 days. The restoring of sea surface salinity is a common method used to prevent the ocean salinity from drastically drifting away from the observed ocean state (Steele et al., 2001). Sea surface salinity restoring compensates for a mismatch between freshwater forcing data (e.g., precipitation and runoff) and model physics. In the absence of restoring the model drift is arbitrary, depending on the combination of forcing data set and model physics. Parametrization of river runoff is employed using negative salt fluxes proportional to seasonal climatologies of runoff for each of the major rivers which follows the AOMIP protocol (Holloway et al., 2007). The model is driven with daily atmospheric forcing from 1948 to 2013 (NCEP/NCAR reanalysis(Kalnay et al., 1996])). NAOSIM has been used successfully in a number of applications focusing on Northern Sea circulation (Karcher et al. 2008, Gerdes et al. 2005) and tracer dispersion (Karcher et al. 2004; 2012). It also has been used for studies identifying worst case locations for radioactive releases in the Nordic Seas (Brown et al., 2016a; Kauker et al., 2016) and contributing to an environmental impact analysis of a potential release form the Russian submarine K-27 (Hosseini, et al., 2017; Karcher et al., 2017).

This work reported upon here encompass marine dispersion of potentially released soluble radionuclides arising offshore from a hypothetical, modelled source of radioactive substances transported from Andreeva Bay to Murmansk, both areas being close to the Norwegian border. Sediment interaction has not been considered; the half-life of relevant tracers has been assumed to be much longer than the modelled dispersion period. The experiments performed encompass a continuous release of 1 TBq/year into the surface layer (0-20m) over the time periods:

A) January 1998 – January 2001

B) January 2007 – January 2010

C) January 2010 – January 2013

The period A January 1998 to January 2001 was chosen because of the exceptional duration of westward flow in the first year. Periods B and C were chosen as more realistic periods from the recent past, with conditions in the Barents Sea more typical for the last decade. These periods also exhibit short events of westward flow. Data was stored as monthly means of the tracer concentration in the common NetCDF format. A web-based database management tool, developed by OASys, was prepared to facilitate interrogation of the data based on geographical and temporal information for each of the experiments.

2.3.2 Selection of input data for use in the subsequent environmental impact assessment

A point was chosen in the marine environment that would yield the most elevated activity concentrations of radionuclides in seawater. The time series data were extracted from the underpinning hydrodynamic modelling results database provided at monthly time intervals using the above-mentioned database

management tool as described elsewhere (Hosseini et al., 2016). Surface concentrations of ^{137}Cs and ^{90}Sr in seawater were selected for an area encompassing the most elevated levels associated with the main plume of contamination for the release scenarios. While these data might correspond to a single grid cell in the modelling domain, the spatial averaging involved was nonetheless quite substantial covering an area of approximately 900 km^2. A spatial averaging of this magnitude might over-compensate for the migratory/peripatetic nature of the animal and fish species covered (Sazykina, 1998 and Wienerroither et al., 2011). However, no higher resolution was available for the model. This observation provided the rationale for considering the surface water only (to a depth of 10 m) in the model output, and for which activity concentrations were at a maximum, to characterize more robustly the potential levels in the environment that could be attained for the release. For consistency, and to address similar concerns regarding spatial averaging, surface water data were also used for the human assessment.

2.3.3 Atmospheric-terrestrial advection dispersion modelling

For the estimation of the atmospheric transport of radionuclides to and deposition over Norway, a decision was made to use earlier simulations performed as part of an environmental risk assessment involving the analysis of radionuclide release and dispersion from the Russian nuclear submarine K-159 (Hosseini et al. 2017). This decision was based on considerations related to the proximity of the two locations (Andreeva Bay and sinking site of the submarine) and the fact that, for any new set of simulations, changes regarding prevailing wind-fields, leading to worst case radionuclide deposition conditions in Norway, would be expected to be minor. A regional weather model could hence be suitably adopted from previous simulations undertaken for K-159.

The model used for simulation of the atmospheric dispersion is called SNAP (Severe Nuclear Accident Program). SNAP is a Lagrangian particle model which was developed at the Norwegian Meteorological Institute, MET (Bartnicki et al., 2011) to simulate atmospheric dispersion of radioactive debris in an emergency situation. The SNAP model has been run with a generic source term twice a day for a period between 1980 and 2012, using the meteorological database NORA10-EI (Reistad et al., 2011). This resulted in a database of depositions containing more than 24 000 deposition maps over northern Europe with a resolution of approx. 11 km. One additional argument for reusing these deposition maps has been the low resolution of these maps. In Fig. 4, the current position of the submarine and the envisaged route of Rosita is shown. However, with regards to Norway a worst-case scenario would be an accident at Andreeva Bay, which is much closer to the Norwegian border. The difference in proximity of release points has been accounted for by conducting some SNAP exploratory simulations, based on release from the Andreeva Bay location, and their comparison with previous results for K-159. The cursory investigation showed that the difference with regards to deposition in Norway, as a result of Andreeva Bay being closer, would be at maximum 3 times the value associated with an accident at the sinking site of the K-159 submarine. Hence, a factor of 3 has been applied to ensure that conservatism is preserved in the reported estimations.

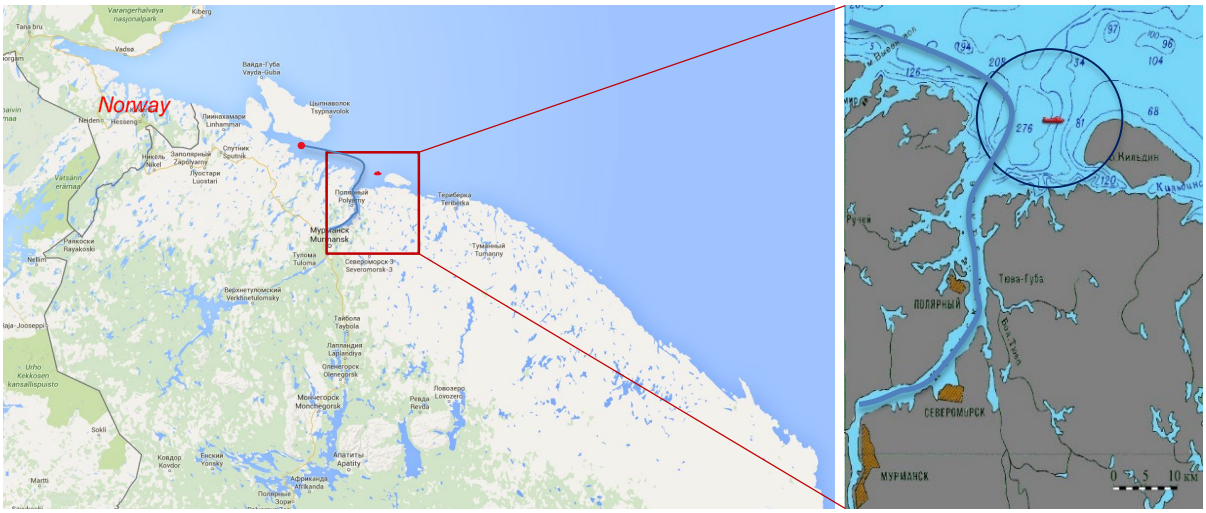

Figure 4: The current position of the submarine K-159 and the envisaged route of Rosita from Andreeva Bay to Murmansk. The circle in the enlarged part has a radius of about 11 km which is equal to resolution of the deposition maps used.

From the obtained deposition maps, only those with deposition over the Norwegian mainland were analysed, and the cases with the largest total deposition to Norway have been selected for more in-depth investigation. For these calculations a possible accident scenario considering a release of 220, 180 and 26 TBq of ^{137}Cs, ^{90}Sr and ^{85}Kr, respectively, to the atmosphere is assumed. The release height is up to 100 m and it was assumed to be short – one hour, in the form of radioactive particles. Based on these runs, a worst case was identified, and maximum depositions and time integrated air concentrations were estimated.

2.3.4 Modelling transfer of radionuclides in food-chains

For the purpose of deriving activity concentrations in representative plants and animals and for human foodstuffs, food-chain models have been applied. For convenience, these have been split into marine (Appendix A) and terrestrial models (Appendix B).

The suite of equations describing the systems (as described below) has been constructed within the modelling platform software ECOLEGO-6. ECOLEGO is a simulation software tool that is used for creating dynamic models and performing deterministic and probabilistic simulations. Further details are reported in Avila et al. (2005).

Result of simulations from marine dispersion models, as described above in Section 2.3, have been provided in the form of a continuous release of 1 TBq/y over a 3-year period. Our outputs from the model in Bq/l (for a generic radionuclide), therefore, correspond to this unit release rate and need to be scaled accordingly.

To make the employed source term inputs compatible with the way the hydrodynamic model was set up, it was assumed that the activity was released at a constant and continuous rate over a 3-year period. A 'scaling factor' was thus derived, by dividing the total release of a given radionuclide (as specified previously) by 3 years. This scaling factor was then applied to every determination of activity concentration for the same radionuclide for every time point. The transfer of contaminants to marine plants and animals is often estimated using concentration ratios (or factors) as described elsewhere (IAEA, 2004; IAEA, 2014). However, the applicability of such parameters is more suited to situations when steady-state conditions

are prevalent as oppose to conditions under which environmental activity concentrations are changing rapidly with time. In these latter cases, dynamic models are more appropriate for determining biological transfer (Vives i Batlle et al., 2008). For this reason, marine food-chain models were applied (Appendix A) to estimate activity concentrations of ^{90}Sr and ^{137}Cs in representative aquatic species.

A terrestrial food-chain model was used to provide input for both the derivation of ingestion doses for humans and for the assessment of doses to wild plants and animals. The approach follows closely the methodologies adopted in quantifying the impact of hypothetical releases arising from the sunken nuclear submarine K-159, the details of which can be found elsewhere (Hosseini et al., 2017).

In view of available data, it was most appropriate to split the modeling into flora (wild grass/grasses, herbs and shrub) and fauna (deer/herbivorous mammal and rat/burrowing mammal) partly based on the classifications given in UNSCEAR (2008). More details regarding the approach taken and modelling works conducted to account for the transfer of contamination along the considered terrestrial food chains can be found in Appendix B.

2.3.5 Doses to humans

Once activity concentrations are derived, models are required to derive dose estimates for both a representative person and representative plants and animals. Standard methodologies were used for the calculation of human exposures (see e.g. IAEA, 2003) from various exposure pathways such as:

- → Ingestion from contaminated foodstuffs
- → Inhalation of radionuclides
- → Exposure arising from a passing plume of contamination - cloud-shine
- → Exposure from contaminated soil or shore sediments

The equations expressing the total annual effective dose from the above pathways is given in Appendix C. The human dose assessment has been spilt into 2 main parts – the first relating to the local region in proximity to the release location for the Andreeva accident scenario and the second for Norwegian territory.

For a representative person on the Kola Peninsula, it was assumed that ingestion of marine products constitutes the dominant exposure pathway. In earlier work and in this regard, IASAP (International Arctic Seas Assessment Project – IAEA, 1998) considered a representative of the average local Russian population (using local marine food products). This group was located on the Kola Peninsula. The dietary habits postulated for these populations were:

- → Sea fish, 50 kg/a (assumed to have been caught in the Barents Sea)
- → Molluscs, 0.5 kg/a
- → Crustaceans, 1 kg/a

The same dietary data has been used for the calculations presented in this report. The activity concentrations of ^{137}Cs and ^{90}Sr in marine biota have been derived using the marine food chain models described in Appendix A using time series radionuclide activity concentrations in seawater as described above.

For a representative person in the European context and with respect to marine pathway transfer, a high rate consumer of seafood was considered. The EFSA (European Food Safety Authority) Comprehensive European Food Consumption Database (EFSA, 2011) has been used as a source of dietary information. It is still necessary to consider a representative person in Norway. Pragmatically, this may be considered to be

a high percentile consumer from the statistics based on the entire country. Consumption rates were provided for fish and seafood of 63 g/d and 250 g/d for an average person and person in the 99th percentile, respectively (Hosseini et al., 2017). The 99th percentile has been selected for subsequent dose calculations. Since no differentiation is made between fish and seafood in statistical data for the dietary information, the assumed breakdown has been taken as 50 % fish and 50% crustacean and molluscs (the latter forming equal components of their 50 %). This may seem somewhat arbitrary and differs from Hosseini et al. (2017) where the diet was assumed to consist of 100 % fish but allows for the inclusion of marine foodstuffs, in the dose calculation, that may be potentially more contaminated than fish (cf. activity concentrations of radionuclides in molluscs and fish in various figures in this report). For consumers of fish and seafood, fish tends to form the predominant dietary component as evidenced by the Kola Peninsula representative person (see above and IAEA, 1998) and as such our breakdown of the diet has been selected to reflect this observation. The activity concentrations in seafood have been obtained via the kinetic models described in Appendix A.

In view of uncertainty regarding where the marine organisms have been prior to capture, a conservative assumption was made that they were caught in a small area corresponding to locations where radionuclide activity concentrations were at a maximum. The time series data for radionuclide activity concentrations in seawater for this area, from 3-dimensional hydrodynamic modelling, has been taken as input to food-chain transfer models. The output from the modelling work is in the form of activity concentrations in organisms with time. For the sake of conservatism, the maximum values from these data series were used in human dose calculations.

In considering exposure due to consumption of terrestrial foodstuffs, the representative person was considered as consumer of natural products in high deposition areas in Finnmark exposed to initial plume and deposition For the sake of conservatism, the maximum values from model simulations for the time integrated activity concentrations of radionuclides in air over Norwegian territory (in Finnmark) were used for inhalation and cloud-shine dose estimates applying the equations given in Appendix C (Equations C-2 and C-3). Exposure from contaminated soil was derived using the maximum deposition levels of radionuclides in Finnmark County. For this, it was conservatively assumed that a person is found in continual contact with contaminated soil over a 1-year period. The reality, even in the absence of orders to shelter or evacuate, would be that individuals are shielded from ground contamination for prolonged periods as people spend a substantial fraction of time indoors. Finally, ingestion doses for people have been derived using various assumptions concerning diet.

The kinetic model described in Appendix B was used where possible to derive activity concentrations in various foodstuffs. The maximum deposition levels of radionuclides in Finnmark County have been used as input to the model and appropriate activity concentration from the time series data generated in this process are then used for subsequent ingestion dose calculations. Further details concerning the use of dietary surveys in the assessment and underlying assumptions can be found in Hosseini et al. (2017).

2.3.6 Doses to biota

Once activity concentrations in environmental media and biota were collated and calculated, dose-rates were derived through application of the ERICA Tool (Brown et al., 2008). A selection was made of representative organisms in line with the guidance given in (ICRP, 2008). For our study, sea mammal (seals), seabirds, crustaceans, molluscs and fish were considered for the marine environment whereas a large mammal, small burrowing mammal and shrub were considered for the terrestrial environment. The basic underlying equations utilize activity concentration data in order to derive internal (D_{int}) and external (D_{ext}) absorbed dose-rates (in units of μGy/h). The total absorbed dose-rate is the sum of these components, through the application of dose conversion coefficients (DCCs). Further details can be found elsewhere (Hosseini et al., 2016) and in Appendix D.

3 Results

3.1 Advection- dispersion of radionuclides in the environment

3.1.1 Marine dispersion

As expected, release of the soluble radionuclide starting in January leads to a steady dispersion of the contaminant to the east, spreading a bit southeastward towards the Russian coast and to the north, for all three experiments (Fig. 5, 7, 9). The major pathways are developing into a split plume with one branch entering the Kara Sea via the Kara Strait, and a second branch moving northeast along the coastline of Novaya Zemlya (Fig. 5, 7, 9). For all experiments, once the dispersed contaminant has reached the frontal zone to the Arctic waters in the northern part of the Barents Sea, part of the contaminant is mixed into these Arctic waters and is carried to the west towards Svalbard. Three years after the start of the release, the tongue of contaminated waters reaching Svalbard is evident in all three experiments (Fig. 5, 7, 9). In the central Barents Sea, some westward spread of the contaminant occurs at an earlier stage, a few months after start of the release, driven by the westward flow. However, the short duration of these westward drift periods are not long enough to allow dispersion far into Norwegian waters. Concentrations stay low, even for the case of the extended period of westward flow in 1998, concentrations above 10^{-6} Bq/m^3 barely cross the 30ºE longitude line (Fig. 5a).

The situation for the southern Barents Sea, just westward to the release, is somewhat different. Here the front between contaminated and uncontaminated water is strongest, the large spatial gradients leading to large differences in the contamination by just 50 km difference in location. A timeseries of surface water concentration (0-20 m) close to Vardø reveals concentrations up to 0.8 x 10^{-2} Bq/m^3 in the late summer of 1998, a few months after start of the release (Fig. 6). When it comes to local details of the flow we must ask for caution with the results of the present model. Local flow features not resolved by the model, plus tidal mixing in the area, may lead to higher concentrations than those simulated here, in close proximity to the front. Timeseries of the concentration in the surface waters (0-20m) for the central Barents Sea near 73ºN 30ºE (Fig. 6b) show the arrival of the westward drift signal from 1998 with 0.5 10^{-6} Bq/m^3 also in late summer. In contrast, the temporal development on the southeastern tip of Svalbard, near Edgeøya (Fig. 6) visualizes a pulse-like arrival of concentrations reaching the maximum 0.3 x 10^{-6} Bq/m^3 three years after start of the release. However, concentrations might keep on rising in the period after the simulation stopped.

For the period January 2007 to January 2010, peak concentrations close to Vardø reach 0.2 x 10^{-2} Bq/m^3 for one month in summer 2007 (Fig. 8a). For this period the peak concentrations in the central Barents Sea near 73ºN 30ºE (Fig. 8b) occur in summer 2008. In late 2009, near the end of the integration, the highest concentration close to Edgeøya (Fig. 8c) is about 0.2 x 10^{-5} Bq/m^3, again at the very end of the 3-year integration, so we might expect a continued period of contamination.

For the latest release period, January 2010 to January 2013, we find a rather regular pulse of increased concentrations each summer near Vardø, highest in the first summer of 2010, while increasing concentrations occur each of the three summers in the central Barents Sea (Fig. 10b). For Svalbard (Edgeøya) (Fig. 10c) the situation is similar to the other periods, with a maximum of the concentrations at the end of the simulation.

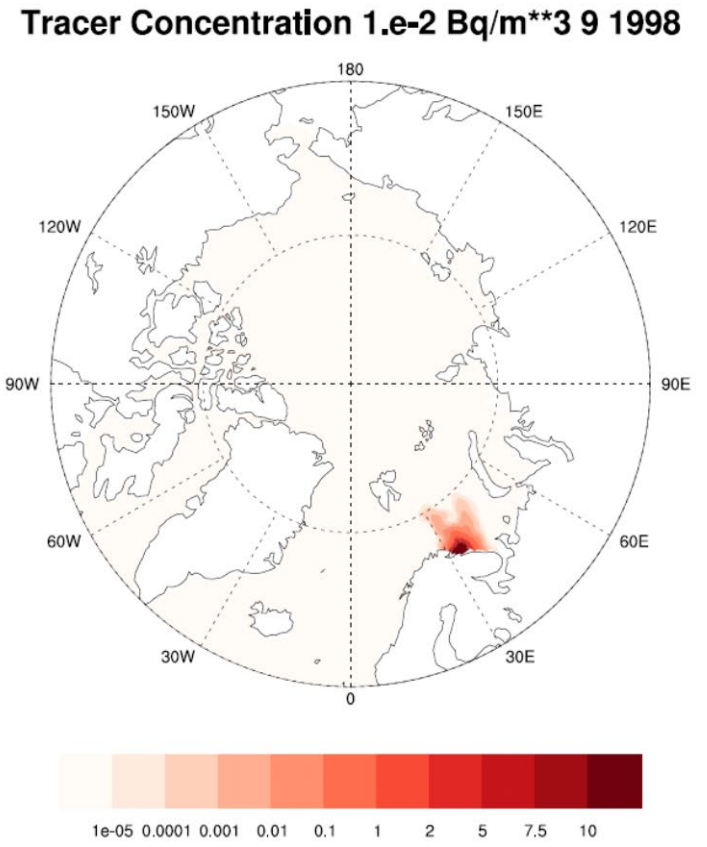

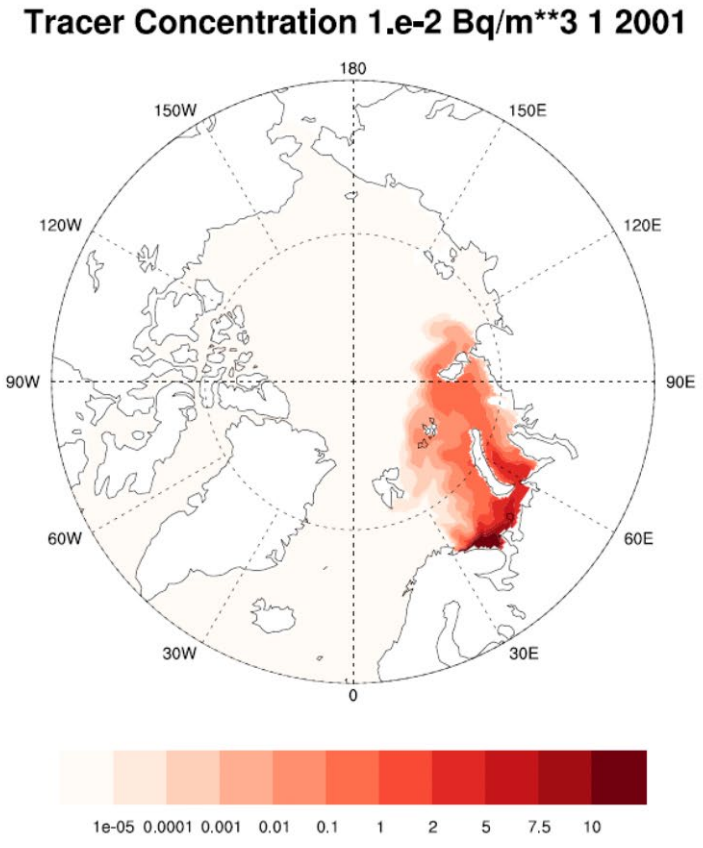

b)

Figure 5: Experiment A: 1/1998-1/2001, Surface (0-20m) concentrations in September 1998 (top) and January 2001 (bottom) after continuous release of 1 TBq/y off Murmansk in 10^{-2} Bq/m^3.

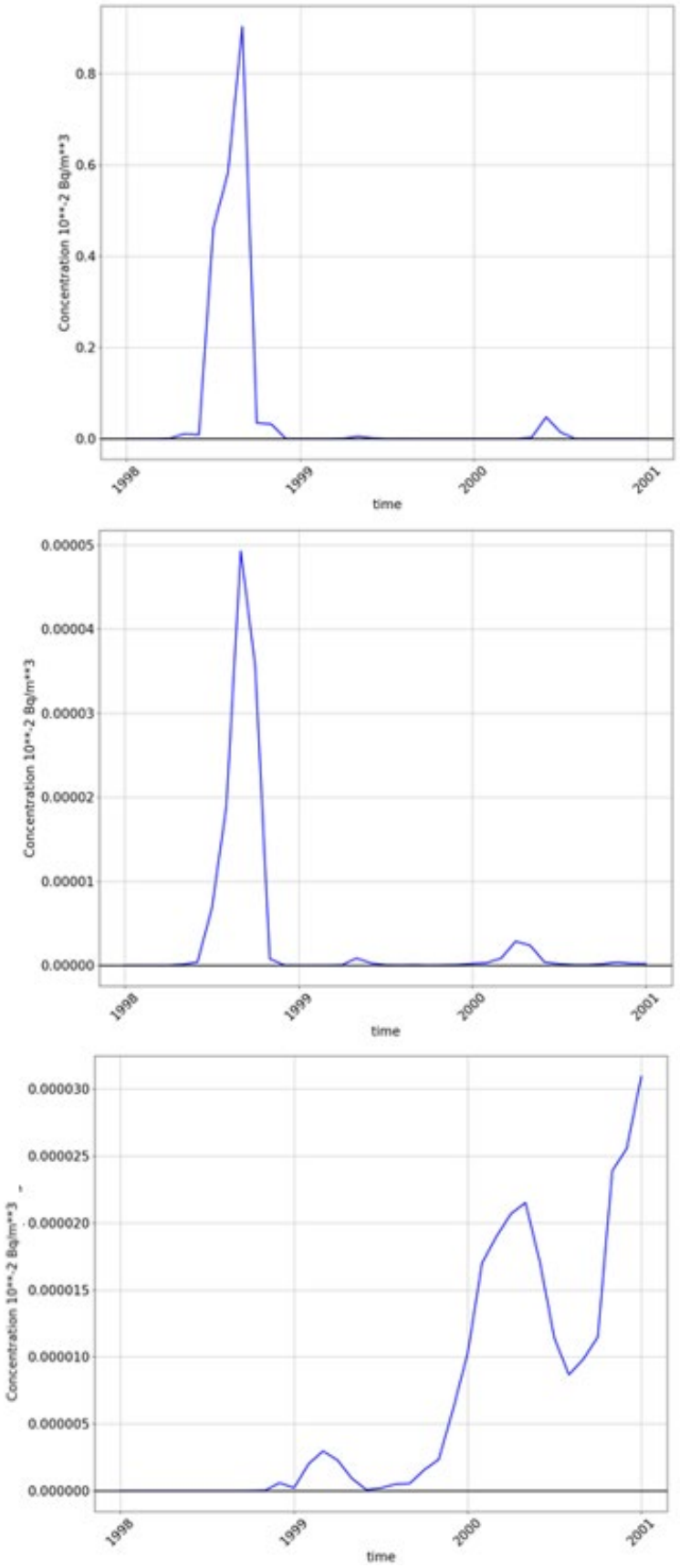

Figure 6: Concentration of the radionuclide (10^{-2} Bq/m^3) in surface water (0-20 m) for Experiment A (1/1998 – 1/2001), just offshore of Vardø.(top), southern Barents Sea, near 73ºN 30ºE (middle) and at the southeastern tip of Svalbard near Edgeøya (bottom).

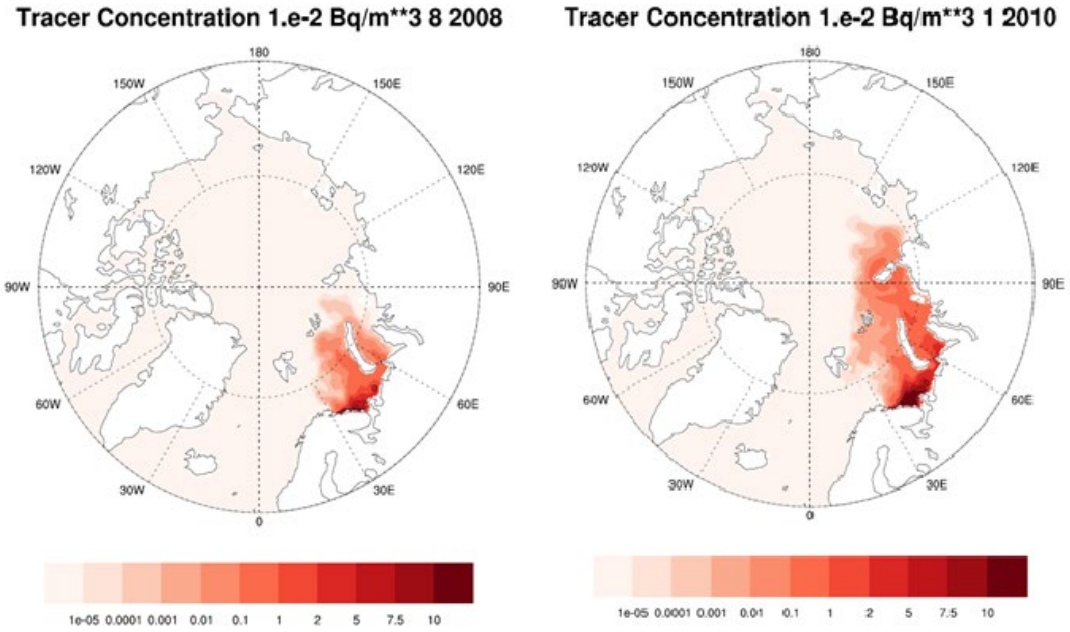

Figure 7: Experiment B: 1/2007-1/2010, Surface (0-20 m) concentrations in August 2008 (left) and January 2010 (right) after continuous release of 1 TBq/y off Murmansk in 10^{-2} Bq/m^3.

As considered in more detail above, it appears that in all cases, i.e. three simulation periods, the dominant flow, and thus dispersion, happens to be East-Northeast, with periods of a few weeks up to a few months of westward flow in the southern and central Barents Sea. This leads to a strong front between contaminated and uncontaminated waters on the western flank of the dispersion plume, which is located very close to, or moving a short distance beyond, the Norwegian-Russian border. Thus, highest concentrations in Norwegian regions can be expected near Vardø, when the front moves westward for some weeks to months. Further north in the Barents Sea, when the contaminated plume reaches beyond the front to the Arctic waters which move west-southwest, contaminant loaded water is carried towards Svalbard. This happens in year 3 after the release has started.

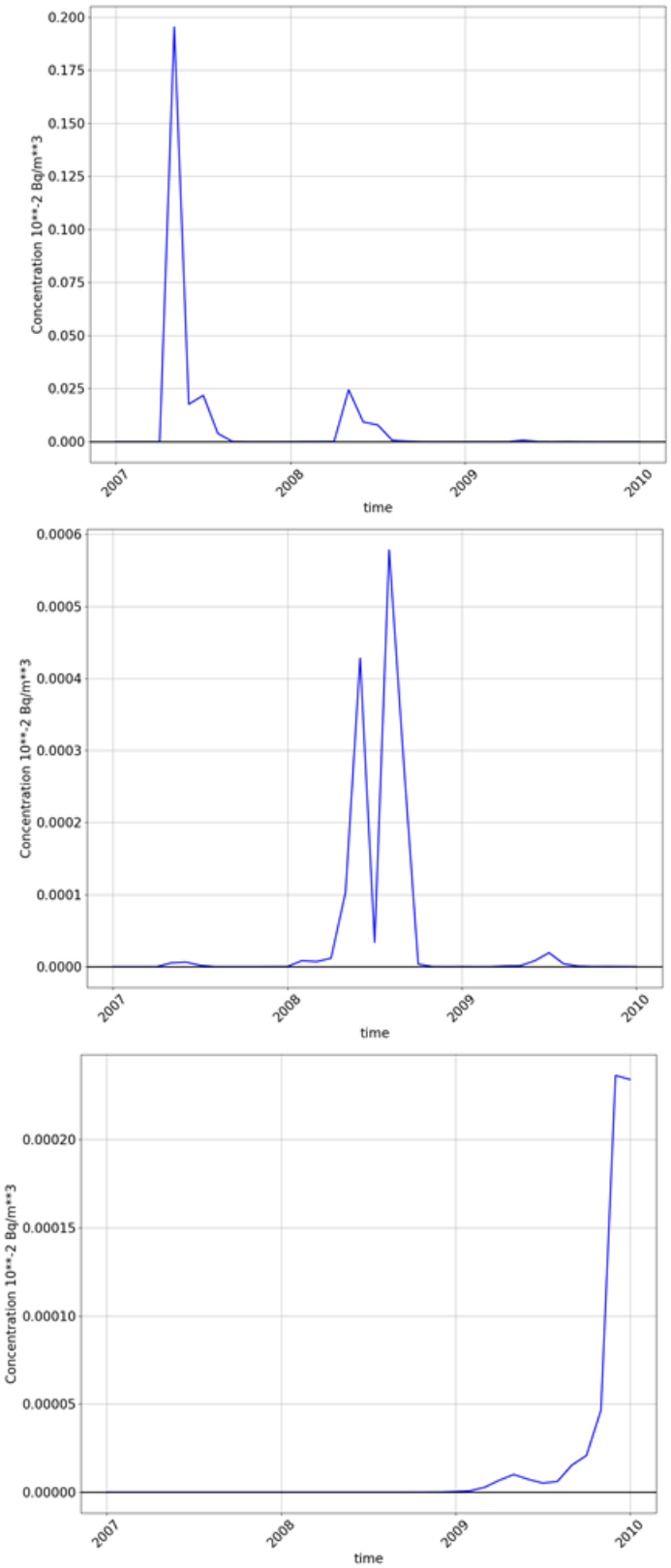

Figure 8: Concentration of the radionuclide (10^{-2} Bq/m^3) in surface water (0-20 m) for Experiment B (1/2007 – 1/2010), just offshore of Vardø (top), southern Barents Sea, near 73ºN 30ºE (middle) and at the southeastern tip of Svalbard near Edgeøya (bottom).

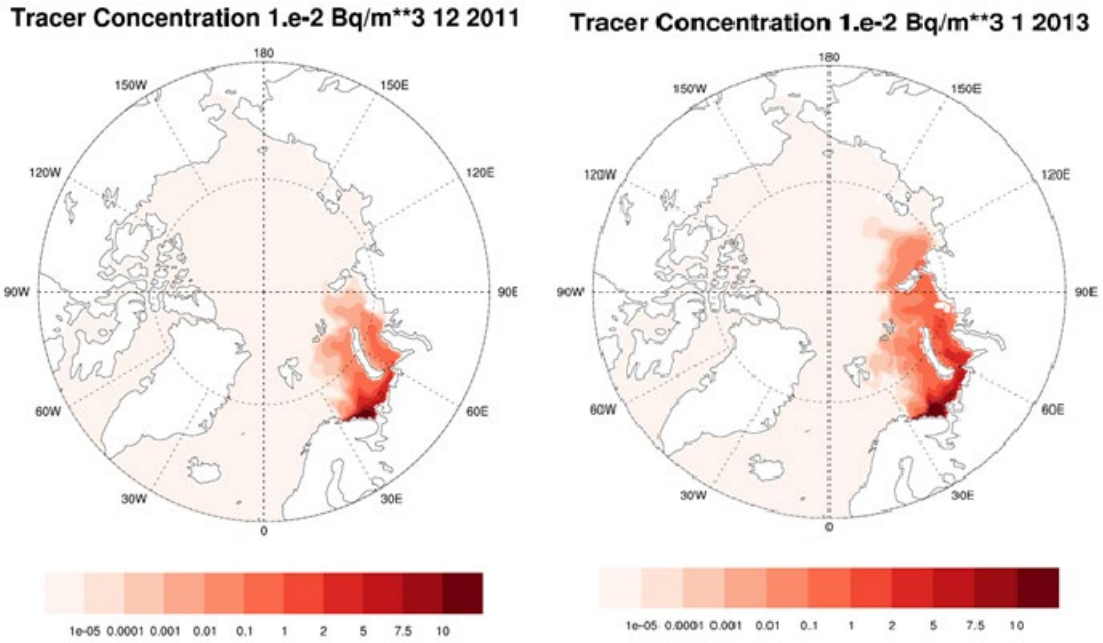

Figure 9: Experiment C: 1/2010-1/2013, Surface (0-20 m) concentrations in December 2011 (left) and January 2013 (right) after continuous release of 1 TBq/y off Murmansk in 10^{-2} Bq/m^3.

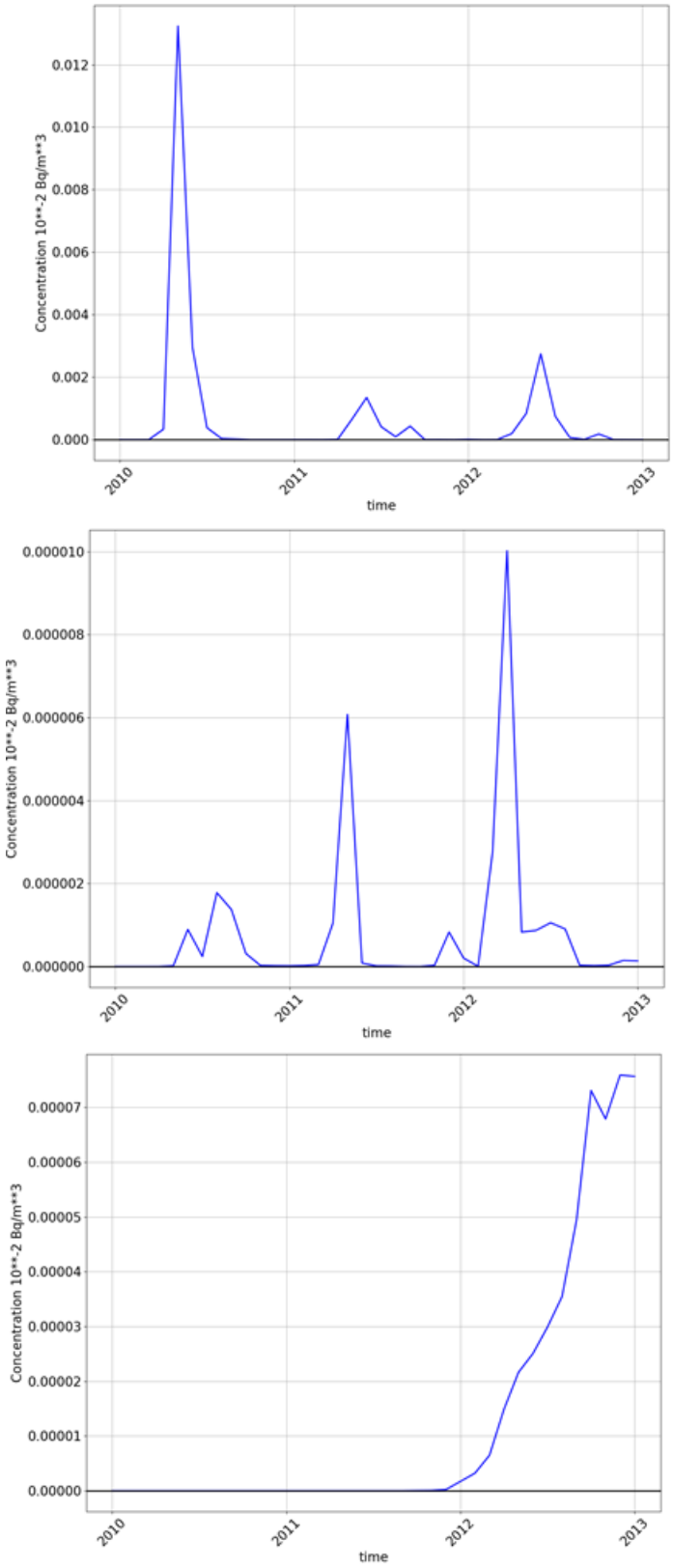

Figure 10: Concentration of the radionuclide (10^{-2} Bq/m^3) in surface water (0-20 m) for Experiment C (1/2010 – 1/2013), just offshore off Vardø(top), southern Barents Sea, near 73ºN 30ºE (middle) and at the southeastern tip of Svalbard near Edgeøya (bottom).

3.1.2 Terrestrial advection-dispersion modelling results

The maximum total deposition to Norway for all model runs covering 33 years of bi-daily runs resulted in a ^{137}Cs and ^{90}Sr deposition of 97 and 79 TBq, respectively. The value for ^{137}Cs can be compared to total fallout of ^{137}Cs over Norway after the Chernobyl accident of 2300 TBq (Henriksen and Saxebøl, 1988). The absolutely worst case with respect to deposition over Norway can be found in one of the model runs (on 1988-07-22 with release between 06-07 UTC), resulting in a deposition where more than half of what has been released ends up in Norway (54%). More on model runs, assumptions made, and the selection of worst cases related to highest deposition in Norway can be found in an earlier report (Hosseini et al. 2017).

3.1.3 Activity concentrations in marine organisms for hypothetical releases

Activity concentrations of ^{137}Cs and ^{90}Sr in marine organisms, resulting from releases into the marine environment for a seawater circulation pattern corresponding to that occurring in the period January 1998 – January 2001, are shown in Fig. 11.

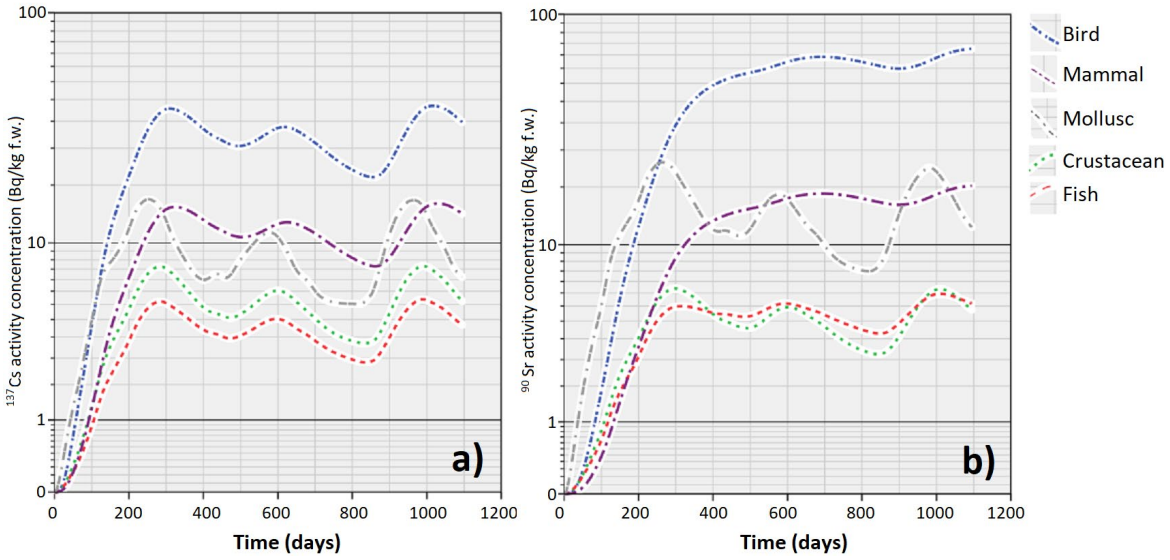

Figure 11: Activity concentrations of ^{137}Cs (Bq/kg f.w.) and ^{90}Sr (Bq/kg f.w.) in marine organisms with time for a release of 220 TBq ^{137}Cs and 180 TBq ^{90}Sr occurring over 3 years with oceanic circulation regime for inputs starting in 1998.

The activity concentrations of ^{137}Cs in marine organisms (Fig. 11) do not exceed 50 Bq/kg fresh weight at any time during the 3-year simulation period. The highest levels are predicted to occur in seabirds, for which ^{137}Cs activity concentrations fluctuate between 20 and 50 Bq/kg, once the system has attained a quasi-steady-state. Nonetheless, given the limited empirical datasets underpinning the biokinetic models for seabirds, these estimates should be considered as being quite uncertain. Cs-137 activity concentrations are relatively low for fish attaining peak levels only slightly in excess of 5 Bq/kg once 280 days have elapsed and oscillating in magnitude in proximity to this value for the remaining simulation period.

An alternative to applying a biokinetic model, as illustrated above, would have been to apply concentration factors, CFs, to seawater activity concentrations as recommended elsewhere (IAEA, 2004). For the particular case illustrated in Fig. 11, ^{137}Cs activity concentrations in seawater were predicted to fluctuate between 0.04 and 0.13 Bq/l (following the initial period of increasing values). Applying the recommended CF from IAEA (2004) to these values would result in an activity concentration in fish falling between 4 and

13 Bq/kg. These are predictions that are commensurate with levels determined via the application of a biokinetic model and suggest that the simpler approach, i.e. using CFs, may have sufficed in providing a reasonable indication of food-chain transfer in this case. Nonetheless, we contend that the validity of the biokinetic model is greater and that the smoothing of extreme values, noting the peak for the biokinetic model output for ^{137}Cs in fish is < 50 % of that derived via a CF, would be a real, observable phenomenon should a substantial release of ^{137}Cs occur.

Despite the hypothetical releases of ^{90}Sr into the marine environment being somewhat lower than those associated with ^{137}Cs, the activity concentrations of ^{90}Sr in most marine organism categories are predicted to be slightly higher than corresponding ^{137}Cs levels. In some cases, notably for mammals and birds, this may be partly explained by slower loss rates of strontium compared to caesium once the radionuclide becomes incorporated into an animal's body. The fact that activity concentrations of ^{90}Sr in mammals and birds are still increasing at the end of the simulation period is indicative of the marine system having not attained a steady state (i.e. equilibration between activity concentrations in seawater and some biota compartments has not occurred within the 3-year simulation period).

The relative transfer of ^{90}Sr to different organism groups shows a similar pattern to that observed for ^{137}Cs with seabirds exhibiting the highest uptake and crustaceans and fish the lowest. The highest activity concentration predicted to occur is in excess of 80 Bq/kg f.w. ^{90}Sr in seabirds and all organism groups exhibit ^{90}Sr activity concentrations in excess of 3 Bq/kg f.w. once quasi-steady-state conditions have been attained.

Activity concentrations of ^{137}Cs and ^{90}Sr in marine organisms, resulting from releases into the marine environment for a seawater circulation pattern corresponding to that occurring in the period January 2007 – January 2010, are shown in Fig. 12 and that for the period January 2010 – January 2013, are shown in Figures 13.

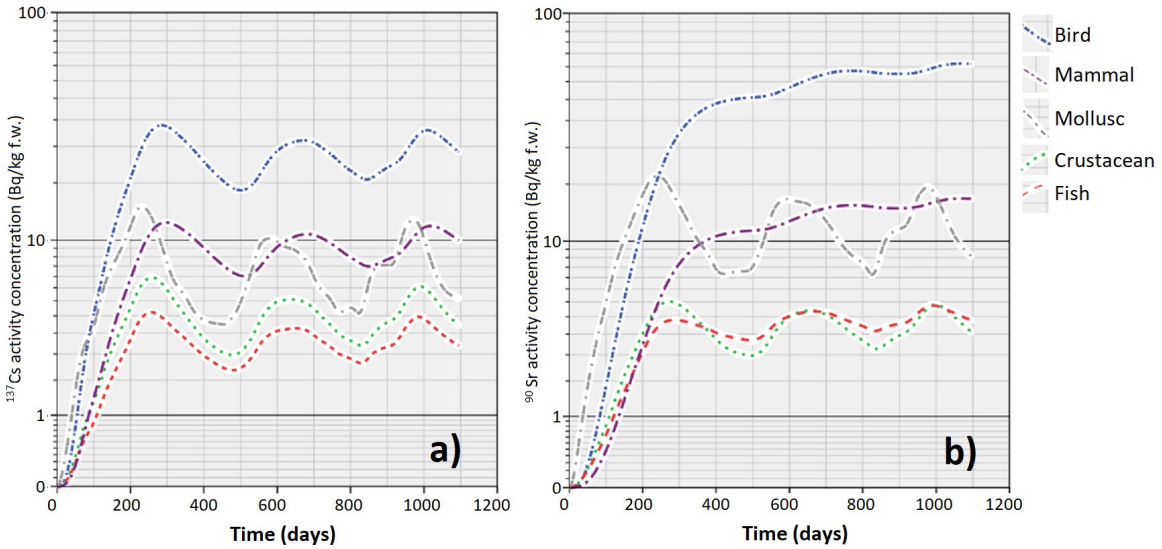

Figure 12: Activity concentrations of ^{137}Cs (Bq/kg f.w.) and ^{90}Sr (Bq/kg f.w.) in marine organisms with time for a release of 220 TBq ^{137}Cs and 180 TBq ^{90}Sr occurring over 3 years with oceanic circulation regime for inputs starting in 2007.

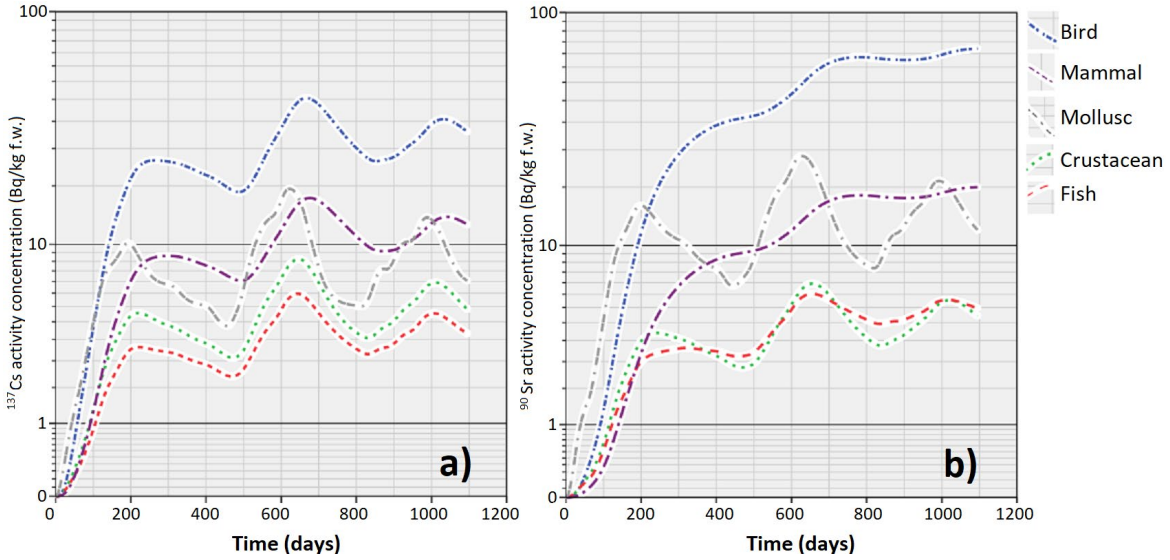

Figure 13: Activity concentrations of ^{137}Cs (Bq/kg f.w.) and ^{90}Sr (Bq/kg f.w.) in marine organisms with time for a release of 220 TBq ^{137}Cs and 180 TBq ^{90}Sr occurring over 3 years with oceanic circulation regime for inputs starting in 2010.

The oceanic circulation regime does appear to make some subtle difference to the form of the temporal evolution of radionuclide activity concentrations in biota, but the absolute levels are generally consistent falling within a few Bq/kg of one another for any given time point. The radionuclide activity concentrations in the organism category 'Mollusc' appear to exhibit the greatest contrast in levels over time in response to different seawater circulation patterns. Whereas activity concentrations of ^{137}Cs in molluscs show peak values occurring at around 200 (simulation) days for the circulation regime starting in 2007, maximum levels occur at around 600 (simulation) days for the circulation regime starting in 2010.

In order to provide some context to the activity concentrations of radionuclides predicted in the marine environment for hypothetical releases from Andreeva Bay, under different oceanic circulation regimes, it is helpful to consider recent levels, in relevant sea areas, based on measurements (Table 1). Reflecting historical inputs from, *inter alia*, atmospheric nuclear testing and western European reprocessing plans (AMAP, 1998) relatively low, but measurable quantities of ^{137}Cs can be determined in seawater in European Arctic seas.

Table 1. Measured activity concentrations of ^{137}Cs in seawater and fish based on samples collected in the Barents Sea and Norwegian Sea in recent years.

Location	Water (Bq/l)	Biota (Bq/kg f.w.)		Reference
Barents Sea	1.6E-03 – 2.0E-03	Fish	<0.3	(Gwynn et al. 2012)
Norwegian Sea	1.1E-03 – 5.9E-03	Fish*	<0.5	NRPA (2011) & NRPA (2015)

*Caught within the coastal waters of Finnmark and Troms.

Clearly, the signal from the specified hypothetical release, in terms of ^{137}Cs activity concentrations in marine food chains, would be easily discernible against existing background levels of contamination. The

predicted activity concentrations of ^{137}Cs in seawater and marine organisms lie at least one order of magnitude above those currently existing in the considered sea areas. Given that ^{90}Sr background activity concentrations in marine organisms from the Barents region have historically been observed to be considerably lower than corresponding levels associated with ^{137}Cs (Heldal et al., 2015) and that radionuclide levels in fish are indicative of ^{137}Cs and ^{90}Sr in other marine organism groups, it is safe to say that a similar argument, regarding the distinctive measurability of (hypothetical) Andreeva inputs on marine food-chains should there be an accident, holds true.

All activity concentrations in marine organisms, as predicted by models for hypothetical release situations, that could be used as food for humans are substantially below the intervention level of 600 Bq/kg as applied for basic foodstuffs in Norway (Liland et al., 2009). Furthermore, the predicted ^{137}Cs activity concentrations in fish, are substantially below the Japanese regulation value of 100 Bq/kg (fresh weight) for sale and human consumption- a limit applied following the accident at Fukushima Daiichi (Buesseler, 2012). Given the highly conservative nature of our assessment and the undoubted highly pessimistic prognosis regarding the contamination of food-chains, the potential requirement for restrictions on the consumption of sea products, should a release during the transport from Andreeva Bay occur, can be summarily dismissed. This contrasts with similar assessments made considering potential releases from the sunken submarine K-159 in the Barents Sea for which Antipov et al. (2015) considered that restrictions, at least in the short term, would plausibly be required.

3.1.4 Activity concentrations in terrestrial food-chains for hypothetical releases

The dynamics of ^{137}Cs activity concentrations in vegetation (shrubs), lichen, small mammals and large (mammalian) herbivores at the location of maximum deposition in Finnmark, following releases associated with a hypothetical accident scenario during transport from Andreeva Bay, are presented in Fig. 14.

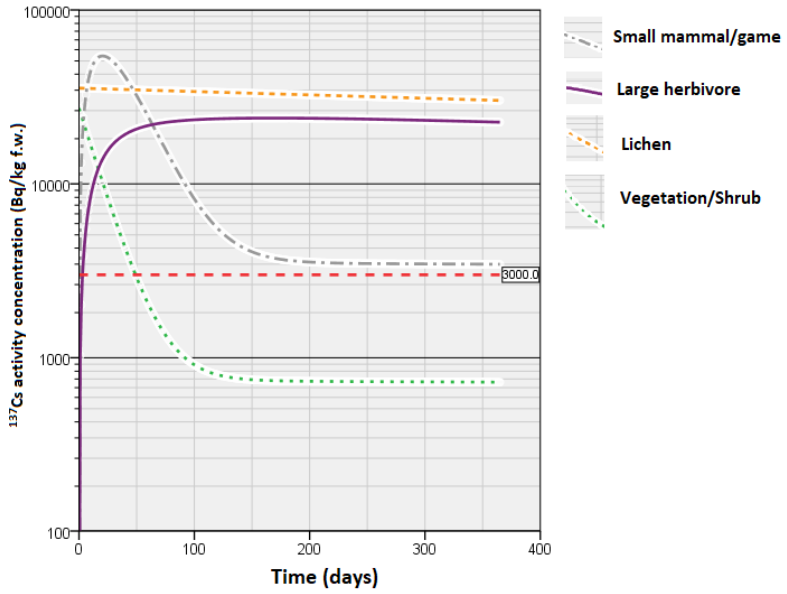

Figure 14: Activity concentrations (Bq/kg f.w.) of ^{137}Cs in selected organisms for the area of maximum deposition in Finnmark for the Andreeva Bay release scenario. The red dashed hortizontal line indicates the current Norwegian intervention level for game/reindeer meat of 3000 Bq/kg.

For lichen and shrubby vegetation, maximum ^{137}Cs activity concentrations are predicted to occur immediately after the hypothesized deposition event with levels declining in the subsequent weeks and months as the radionuclide is weathered from the (above soil-surface) canopies. Initial ^{137}Cs activity concentrations were simulated to be in excess of 27 kBq/kg (f.w.) for shrub and in excess of 35 kBq/kg (f.w.) for lichen primarily reflecting the interception fractions used in model parameterization. The decrease in ^{137}Cs levels with time follow quite divergent trajectories. Whereas activity concentrations in lichen fall slowly, remaining at levels above 30 kBq/kg (f.w.) by the end of the 1-year simulation period, the activity concentrations in shrub decline by a factor of about 40, so that concentrations are substantially below 1 kBq/kg (f.w.) by the corresponding time point. Both small and large mammals exhibit ^{137}Cs activity concentration maxima that occur at a finite time period post deposition. This maximum occurs at 20 days after deposition for small mammals and at around 170 days for large herbivores. The ^{137}Cs activity concentrations in small mammals attain a maximum that is > 50 kBq/kg (f.w.) but this level falls relatively quickly to a value of approximately 3.5 kBq/kg (f.w.) by the end of the simulation period. In contrast, ^{137}Cs activity concentrations in large herbivores exhibit absolute maxima that are lower, approximately 24 kBq/kg (f.w.), but decline much more slowly from peak levels and remain substantially in excess of 22 kBq/kg (f.w.) by the end of year 1.

The terrestrial model applied in the current assessment had been developed earlier (Hosseini et al., 2016; 2017 and Brown et al., 2016b). During this earlier process and to reflect the uncertainty associated with using a relatively untested model, a check for ^{137}Cs large herbivore predictions was made against a more established model developed specifically to look at radiocaesium levels in reindeer following Chernobyl accident derived deposition (see Åhman, 2007). The previous study found some reassuring similarities in terms of the maximum activity concentrations that would be predicted for similar ^{137}Cs deposition inputs to the models. Nonetheless, it was acknowledged that the Åhman model provides an additional advantage by providing a quantification of activity levels in the years following a deposition event. It was further noted by Brown et al. (2016b) that an interesting feature of Åhman's model is the closeness with which the observed high amplitude, approximately sinusoidal form of ^{137}Cs levels in reindeer can be simulated by accounting for factors such as the animal's changing diet and metabolism over the season. From the earlier analysis it was concluded that new peak activities, coinciding with subsequent winter periods, would be expected and that these subsequent peaks might be expected to fall at levels that were not dramatically lower than the initial maximum. In view of our using the same model for this analysis, similar inferences can be invoked for the current assessment.

The activity levels for small (burrowing) mammals and deer can be compared to the current relevant Norwegian intervention level of 3000 Bq/kg f.w for radiocaesium (as applied following the Chernobyl accident) and applicable to, *inter alia*, reindeer and game (Thørring et al., 2010). Clearly, ^{137}Cs activity concentrations in large herbivores (nominally reindeer) are substantially in excess of the intervention level for the virtually the entire simulation period. For small mammals/game, ^{137}Cs levels are much higher than the intervention level in the initial period, i.e. first 100 days or so of the assessment, falling to levels marginally above the intervention level towards the end of the first year. The introduction of restrictions on the consumption of reindeer/game would, therefore, be highly likely, potentially involving various measures such as the dissemination of dietary advice and, for reindeer at least, the use of live monitoring before slaughtering. Although the simulations suggest a fairly rapid decline in ^{137}Cs activity concentrations within the first year, the uncertainty associated with the longer-term predictions would precipitate the need for careful monitoring of the situation. In other words, model prognoses of this type could not be used in isolation to predict for how long any introduced restrictions would need to be retained. Similarly, for shrubs (used as a proxy for berries) restrictions on fruit consumption might foreseeably need to be introduced, at least in the first harvesting season. The highest predicted levels are substantially above the Norwegian intervention level for basic foodstuffs of 600 Bq/kg f.w for radiocaesium (Liland et al.,2009; Thørring et al., 2010).

The dynamics of ^{90}Sr activity concentrations in vegetation (shrubs), lichen, small mammals and large (mammalian) herbivores at the location of maximum deposition in Finnmark, following releases associated with a hypothetical accident scenario during transport from Andreeva Bay, are presented in Fig. 15.

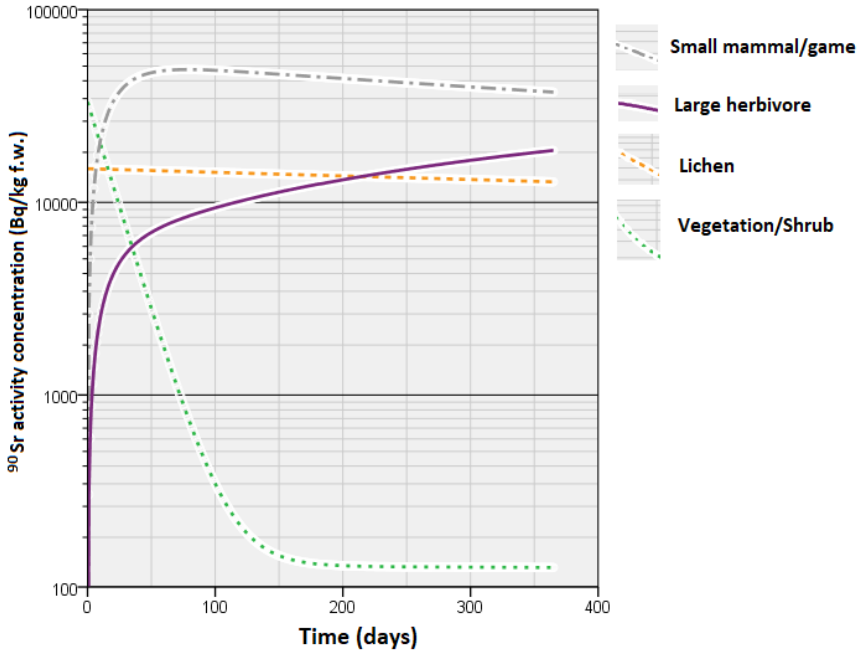

Figure 15. Activity concentrations (Bq/kg f.w.) of ^{90}Sr in selected organisms for the area of maximum deposition in Finnmark for the Andreeva Bay release scenario.

The temporal profiles representing ^{90}Sr activity concentrations in lichen and vegetation/shrub are similar in form to those observed for ^{137}Cs. Both lichen and shrub exhibit maxima, of ca. 33 kBq/kg (f.w.) ^{90}Sr for shrub and 15 kBq/kg (f.w.) ^{90}Sr for lichen, at the start of the simulation but ^{90}Sr levels in lichen decline relatively slowly whereas vegetation levels are predicted to fall relatively quickly attaining levels that are 260 times lower than the start point once 365 days have elapsed (cf. corresponding decrease for ^{137}Cs was ca. 40). The temporal profiles for ^{90}Sr levels in mammals contrast quite distinctly with ^{137}Cs activity concentrations in mammals vs time. The maximum ^{90}Sr of 49 kBq/kg (f.w.) in small mammal is predicted to occur at a time approximately 80 days after deposition, i.e. somewhat later than for radiocaesium, but in contrast to the rapid falloff seen for ^{137}Cs, activity concentrations decline relatively slowly and are still at a level exceeding 37 kBq/kg ^{90}Sr after 365 days of elapsed time. For large herbivores, no steady state appears to have occurred between environmental compartments even following 1 year of simulation as levels of ^{90}Sr are still increasing at this stage. The maximum level at the end of the simulation in large herbivore is approximately 18.5 kBq/kg ^{90}Sr (f.w.). As noted earlier in Hosseini et al. (2016) when applying an earlier version of the aforementioned biokinetic model, there is an expectation that ^{90}Sr will be lost relatively slowly from the body of mammals following assimilation because the radionuclide rapidly becomes associated with bone (see Coughtrey & Thorne, 1983). Once sequestered by bone the retention of radiostrontium within the animal's body can be protracted, reflecting the skeletal turnover of analogous elements such as calcium. This is congruent with the model predicting a continued increasing trend in ^{90}Sr activity concentrations in reindeer towards the end of the simulation.

Nonetheless, Hosseini et al. (2016) also considered the observation of no equilibrium (in ^{90}Sr) being attained over the 1-year simulation period could simply reflect poor parameterisation of the model. For example, in the case of reindeer, the diet and the biological half-lives (for radiocaesium and by proxy conceivably for other radionuclides) are known to vary throughout the year (Åhman, 2007) but these

considerations were not accounted for in the model. Despite the acknowledgment that the configuration of the model is limited after the first few months, it is not unrealistic to expect a continued build-up of ^{90}Sr during later periods. This is based on the assumption that ^{90}Sr is strongly retained on lichen thus leading to a relatively slow decline in levels with time as suggested by Golikov et al. (2004) and the knowledge that lichen do form a large part of the reindeer's diet at some periods of the year. Under such conditions, considerable time would be required to attain anything approaching equilibrium. Having said this, the appropriateness of using an approximately 5 year weathering half-time value for ^{90}Sr may be questionable in view of evidence to the contrary where (more or less corresponding) effective half-times of about 1.0 year for ^{90}Sr in lichen have been apportioned (Skuterud et al., 2005). Although the value of 5 years has been retained for the sake of conservatism, the effect of applying a lower weathering half-time for ^{90}Sr in lichen would be to observe a more rapid attainment of a maximum activity concentrations in reindeer.

3.2 Doses to humans

3.2.1 Doses to humans from marine exposure pathways

Annual effective doses to people representing critical groups from the Kola Peninsula and represented by a high rate seafood consumer in Norway are shown in Table 2.

Table 2. Estimated annual committed effective doses to human for ingestion of marine foodstuffs based on a hypothetical release at Andreeva Bay.

Oceanic Circulation Pattern - period	Annual effective dose (μSv)	Critical Group - Comments
1998-2001	13	Representative person in identified population group in Kola Peninsula, based on ingestion of fish, molluscs and crustaceans
2007-2010	11	
2010-2013	13	
1998-2001	37	Representative person in identified population group in Norway - high rate consumers of seafood
2007-2010	31	
2010-2013	39	

The annual doses fall in the range between 11 to 39 μSv. The doses attributable to high rate consumers of seafood in Norway are approximately a factor of 3 greater than critical groups from the Kola Peninsula, simply reflecting the much greater consumption of seafood in the former group.

These doses may be considered to be low. The radiation dose to the average Norwegian from food and drinking water has been estimated to 0.52 mSv/year from naturally occurring sources (Komperød et al., 2015). Virtually the entire 0.19 mSv/year attributable to the ingestion of fish and shellfish containing artificial and naturally-occurring radionuclides, by the Norwegian population, may be considered to have its provenance in natural sources with ^{210}Po and radium constituting key components. In other words, the

current doses attributable to the ingestion of seafood containing natural 'background' radioactivity for the Norwegian population is approximately a factor of 10 greater than the corresponding hypothetical doses that could arise from releases of artificial radionuclides to Andreeva Bay. The Norwegian population undoubtedly lies at the higher end of statistical compilations for the consumption of seafood across the globe. As considered by Aarkrog et al. (1997), the global mean individual dose from ^{210}Po in seafood (6 μSv) corresponds to about 1 day's effective dose from all natural sources of radioactivity (2.4mSv per year according to UNSCEAR (1993)). So, this contribution from ^{210}Po in seafood alone (noting that this value would undoubtedly be higher for high consumers of seafood in Norway) would be commensurable with the annual dose predictions being made for the hypothetical accident for the marine exposure pathway.

Similarly, reference can be made to various dose benchmarks typically considered within a regulatory context. As noted by Hosseini et al. (2017), in the context of setting criteria to allow or forbid the dumping of radioactive material at sea, the IAEA (1999, 2015) have used a *de minimis* dose of 10 μSv per annum. This effective dose (in tandem with a defined collective effective dose) to a representative person would allow a practice to be exempted from further regulatory consideration. The *de minimis* level specified above provides a robust indication of what might be widely considered to be a trivial radiation dose and as such provides an appropriate benchmark with which the doses calculated in this assessment might be compared. The annual doses calculated for the hypothetical release from the marine exposure pathway, therefore, fall only slightly above a level that is putatively regarded as trivial.

It goes without saying that, the doses fall within the ICRP's reference band, germane to accidental releases of radioactivity, 'below 1 mSv' where a requirement for significant intervention would not be deemed appropriate (ICRP, 2007).

3.2.2 Doses to humans from terrestrial exposure pathways

Annual effective doses to people representing Norwegian critical groups living in a region of maximal deposition (i.e. within Finnmark) are shown in Table 3. It should be noted that the focus of the assessment has been on Norway with no effort placed in assessing doses for locations in greater proximity to the hypothetical release point.

The annual effective dose to a representative person in Finnmark exceeds 20 mSv per year and would be dominated by the ingestion pathway. The finding that the ingestion pathway would dominate the dose in Finnmark is congruent with earlier analyses for submarines K-27 (Hosseini et al., 2016) and K-159 (Hosseini et al., 2017) with scenarios following a salvaging operation and fires. This, however, is not a corroboration of the analysis because the same approach was used in all of these assessments, i.e. the same atmospheric advection dispersion models, food-chain transfer models and dose calculation methodologies were applied. It should be further noted that the 20 mSv calculated assumes no intervention, with the continued ingestion of the most highly contaminated products over a 1-year period. Self-evidently, in the event of a real accident with releases at the (worst case) hypothesized levels, food interventions levels would be exceeded (see discussion above) and critical groups would be controlled from ingesting highly contaminated foodstuffs.

Table 3. Estimated annual effective doses to individuals in identified population group in Norway for various pathways based on releases to atmosphere at Andreeva Bay.

Pathway	Annual effective dose (mSv)
Inhalation	1.36E-02
Cloud shine	4.00E-05
Ground shine	4.60E-01
Ingestion (terrestrial food)	2.07E+01
Total	2.12E+01

Internal doses from terrestrial food products are almost three orders of magnitude greater than the internal doses associated with a high rate fish consumer living in Norway. This clearly illustrates that the overwhelmingly predominant risk to Norwegian populations should an accident involving the transport of SNF from Andreeva to Murmansk would be via an atmospheric transport pathways and terrestrial food-chains.

The total average dose from ionising radiation to the Norwegian population (including medical applications) has been estimated to 5.2 mSv/year with the single highest dose contribution caused by inhalation of radon in indoor air (Komperød, 2015). The hypothetical doses derived in the current analysis are a factor of 4 greater than this value and might therefore be considered substantial.

The ICRP (2007) set a Reference level band of 20 to 100 mSv set for the highest planned residual dose from a radiological emergency and the calculated values within the current assessment fall just into the lower end of the specified range. If doses fall within such a band the ICRP note that consideration should be given to reducing doses, Individuals should receive information on radiation risk and on the actions to reduce doses and assessment of individual doses should be undertaken. In fact, for Norway, if an accident did occur and projected doses were as high as those considered above, reference to prescribed protective measures for the public such as those published in relevant guidance (Nordic Flagbook, 2014) would be required. It is noted in the Nordic “Flagbook” that If the projected dose due to the radiation hazard without any protective measures in higher than 10 mSv then it would be necessary to apply appropriate protective measures.

3.3 Doses to biota

3.3.1 Dose rates in marine organisms

Dose rates in marine organisms for the 3 specified oceanic circulation patterns are shown in Fig. 16. The organisms can be essentially split into 2 groups – pelagic and benthic. The pelagic group, comprising of (pelagic) fish, mammals and seabirds, exhibit relatively monotonous dose-rates over time (following the initial increase) reflecting the fact that a predominant proportion of their dose rate is derived from internally-incorporated radionuclides. In contrast, dose-rates for the benthic group, comprising of molluscs and crustaceans, exhibit dose-rates that fluctuate substantially over time. In this case, external exposure dominates, with dose rates in benthic organisms reflecting ambient radionuclide activity concentrations in seawater. This may be an artefact reflecting the assumptions in modelling radionuclide levels in the

organism's habitat, i.e. at the sediment-water interface. Sediment activity concentrations of ^{137}Cs and ^{90}Sr were derived using a k_d, for which instantaneous equilibration between activity levels in seawater and sediment (at the seabed) are assumed. Not only would radionuclide activity concentrations in sediment not be expected to attain steady state conditions with radionuclide levels in the overlying water column so quickly (i.e. non-instantaneously), there is, arguably, an additional conservatism that has been introduced by using activity concentrations in surface waters. For a surface release of radionuclides, as modelled in this work, radionuclide levels in seawater in contact with the seabed might be expected to exhibit substantially lower levels than those observed at the surface.

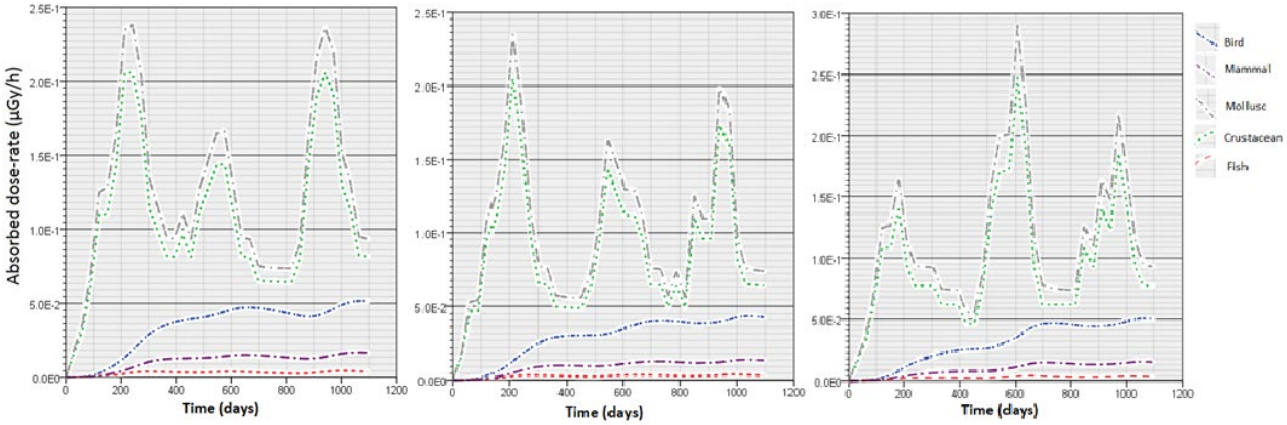

Figure 16. Dose-rate (µGy/h) for fish, molluscs, crustacea, mammals and seabirds for the oceanic circulation pattern of 1998 (left), for the oceanic circulation pattern of 2007 (middle) and for the oceanic circulation pattern of 2010 (right).

The highest dose-rates are observed for the benthic group, with crustaceans and molluscs exhibiting dose rates often exceeding 0.1 µGy/h over the course of the simulation and, in the most extreme case, attaining exposure levels exceeding 0.25 µGy/h for a short period in the case of the circulation pattern from 2010. The levels of exposure of pelagic organisms are substantially lower, by contrast, and only slightly exceed 0.05 µGy/h for a short period of time in the case of seabirds and the circulation patterns for 1998 and 2010. Dose rates for other pelagic organisms are relatively low for all circulation patterns, with fish exhibiting exposures substantially below 0.01 µGy/h.

The effect of circulation pattern is quite subtle. All 3 current regimes, starting in 1998, 2007 and 2010, exhibit 3 distinct maxima in the benthic organism's dose rates and these occur approximately during the same time periods. It is only really in the absolute levels of exposure that differences become more evident. The highest dose-rates for benthic organisms for the 1998 circulation pattern are observed during the 1st and 3rd periods of elevated exposure and for which levels are approximately commensurate. In contrast, the highest exposure for the 2007 circulation are observed during the 1st peak and that for the 2010 circulation for the 2nd peak.

There are two common ways to contextualize dose-rates to wild organisms (Brown et al., 2004a). One is to compare the dose rates to natural background radiation, arising from the presence of primordial (and sometimes cosmogenic) radionuclides in the environment and the other is to compare against benchmarks that inform us about the levels at, or above, which some form of deleterious effect is likely to occur.

Weighted (to account for differences in the magnitude of deleterious effects associated with radiation quality) absorbed dose rates from exposure to naturally occurring radionuclides of 5.8×10^{-1} and 8.7×10^{-1} µGy/h were calculated by Hosseini et al. (2010) for a set of marine organisms comprising of flatfish, crabs and seaweed. The variability associated with these estimates is considered to be substantial, reflecting the

great differences that are often observed in the activity concentrations of naturally-occurring radionuclides in natural systems. For benthic organisms, exposures will be particularly associated with variability in radionuclide activity concentrations in sediments, generally reflecting, in turn, the levels in the source rock from which they were derived, and furthermore the grain size. The maximum dose rates calculated in the present study are substantially lower than the aforementioned dose rates attributed to natural background radiation in the marine environment albeit falling within the same order of magnitude. Most of the dose rates calculated, and most notably for fish, mammals and seabirds, are at least one order of magnitude below the dose rates associated with naturally occurring radionuclides. For this group of pelagic organisms, one can conjecture that the projected dose rates would fall within the variability associated with the exposure of marine organisms, in general, to natural background radiation over a wide geographical region.

With regards to benchmarks, the ICRP (ICRP, 2008) recommend the application of a set of Derived Consideration Reference Levels (DCRLs) for particular categories of Reference Animals and Plants (RAPs) (Fig. 17). These are defined as "*A band of dose rate within which there is likely to be some chance of deleterious effects of ionising radiation occurring to individuals of that type of Reference Animal or Plant (derived from a knowledge of defined expected biological effects for that type of organism) that, when considered together with other relevant information, can be used as a point of reference to optimise the level of effort expended on environmental protection, dependent upon the overall management objectives and the relevant exposure situation.*"

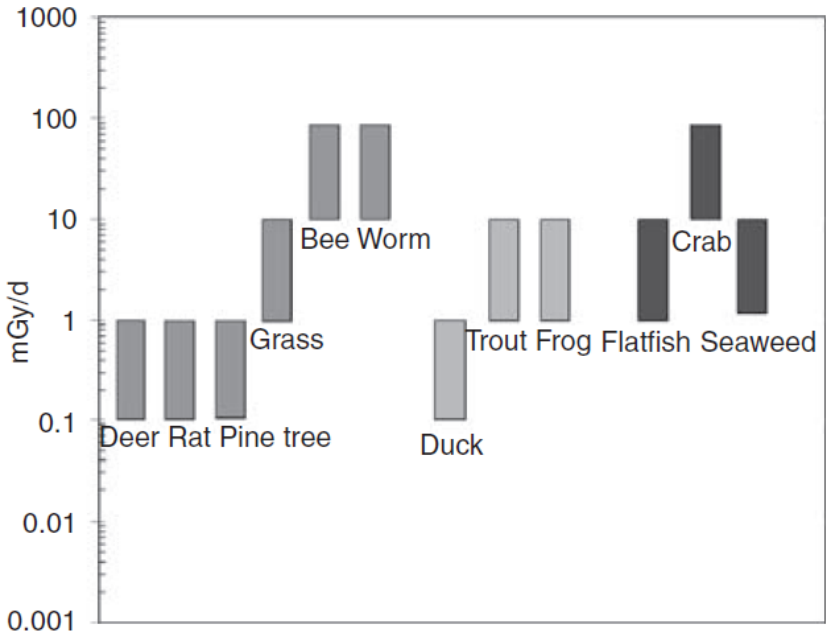

Figure 17. Derived Consideration Reference Levels (DCRLs) for environmental protection for each Reference Animal or Plant (RAP), the RAPs being grouped according to their terrestrial, freshwater, or marine habitat. Reproduced from ICRP (2014).

Although dose-rates for the marine RAPs included in ICRP (2008) have not been calculated explicitly, apart from crustacean/crab, it should be fairly clear that all of calculated dose-rates fall at least two orders of magnitude below the lower end of the DCRLs associated with marine RAPs – 1 mGy/d or 42μGy/h. As such, the dose rates derived in the present study would be far below the threshold above which one might expect to observe deleterious biological effects.

3.3.2 Dose rates in terrestrial organisms

Absorbed dose rates vs time in terrestrial organisms located in the maximum deposition area in Finnmark following an atmospheric release from Andreeva in line with the specification stipulated earlier is presented in Fig. 18.

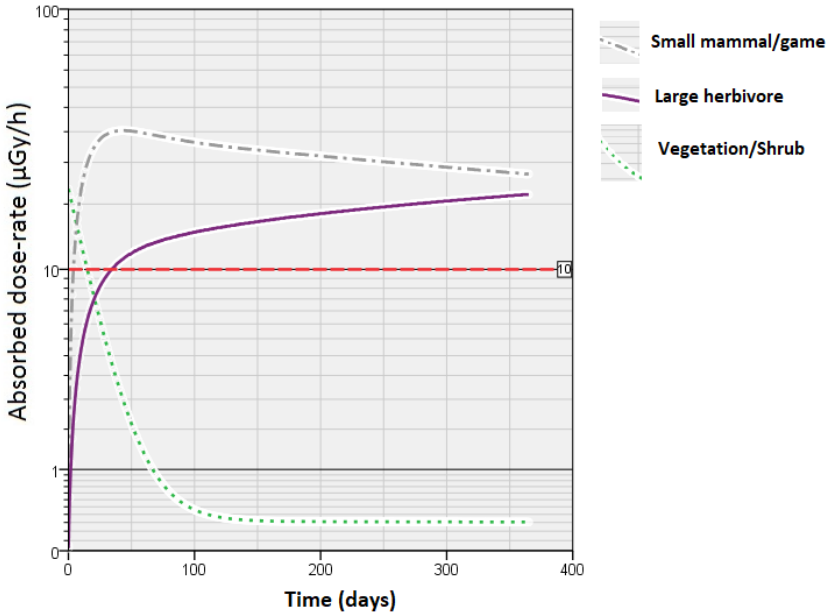

Figure 18. Dose-rate (µGy/h) for terrestrial biota – small mammal/game, large (mammalian) herbivore and Vegetation/shrub – in Finnmark following an atmospheric release from Andreeva. The red dashed horizontal line indicates the ERICA screening benchmark (Brown et al., 2016c).

The absorbed dose rate in vegetation shrub exceed 20 µGy/h at the start of the simulation but decrease rapidly thereafter and fall substantially below 1 µGy/h once 50 days have elapsed. In contrast both small and large mammals exhibit dose rates that increase substantially following the initial deposition event reflecting the time lag for radionuclides to be transferred through the food-chain. Maximum dose rates, exceeding 40 µGy/h, are observed for small mammals within the first 50 days of simulation whereas maximum dose rates for large mammals, exceeding 20 µGy/h, are observed at the end of the simulation period. The fact that dose-rates for large mammals are still increasing at time = 365 days reflects the observation that ^{90}Sr levels have not attained a steady state between environmental compartments as discussed previously. A summarised table for dose rates in terrestrial biota is provided in Table 4.

The calculated dose-rates for all organisms exceed the ERICA screening benchmark of 10 µGy/h at various stages during the course of the simulation. Although strictly applicable to long term planned releases of radionuclides to the environment, the exceedance of this benchmark would lead to a recommendation to provide a more detailed analysis of the exposure of non-human biota. In other words, the predication of environmental dose rates greater than 10 µGy/h dose rate not necessarily indicate any detrimental impact but would be at such a level where the absence of deleterious effect cannot be guaranteed.

Table 4. Maximum activity concentration in terrestrial biota at Finnmark along with the estimated associated dose rates.

Accident location	Maximum activity, kBq/kg (f.w.)			Maximum dose rate (μGy/h)
	Biota	^{137}Cs	^{90}Sr	
Gremikha Bay	Vegetation	2.7E+01	3.3E+01	2.1E+01
	Small mammals	5.4E+01	4.9E+01	4.0E+01
	Deer	2.4E+01	1.9E+01	2.0E+01

Typical background dose rates (from terrestrial primordial radionuclides and excluding inhalation doses from ^{222}Rn) for terrestrial organisms have been reported in the range 0.07 to 0.6 μGy/h (Beresford et al., 2008a). The hypothetical dose rates calculated in the current analyses are therefore at least an order of magnitude greater than the upper end reported in the aforementioned range.

Furthermore, the maximum dose rates for large mammal-deer (ca. 0.48 mGy/d) and small mammal-rat (ca. 0.96 mGy/d) fall directly within the DCRL bands defined in Fig. 17, above. The ICRP (2014) are unambiguous about their recommendations should dose-rates be determined that fall above the DCRL band noting "For existing exposure situations, and emergency exposure situations where control of the source has still not been obtained, if the dose rates are above the relevant DCRL band, the Commission recommends that the aim should be to reduce exposures to levels that are within the DCRL bands for the relevant populations, with full consideration of the associated radiological and non-radiological consequences." On the other hand, the ICRP are more ambivalent about dose rates than fall within the band noting that "*the Commission recognizes that it may be difficult, or impractical, to significantly reduce the concentrations or quantities of radioactive material that exist in the affected environment. If dose rates are within the band, the Commission believes that consideration should be given to reduce exposures, assuming that the costs and benefits are such that further efforts are warranted…*"

4 Conclusions

The inputs for the modelling work of this study have been purposefully conservative with respect to potential inventory, releases, dietary habits and other parameters. The resulting concentrations and doses are expected to represent extreme levels, given an accidental release of ^{137}Cs and ^{90}Sr due to an accident whilst transporting SNF from Andreeva Bay via the sea route to Murmansk. For the marine environment, the highest water concentrations in Norwegian coastal waters would be of the order of 0.2×10^{-2} Bq/m^3 per TBq/year released over a 3 year period. Further north in the Barents Sea it can be concluded that potential additional contamination from the modelled releases is likely to be minimal. All activity concentrations in marine organisms, as predicted by models for hypothetical, conservative release situations, that could be used as food for humans are substantially below the intervention level of 600 Bq/kg as applied for basic foodstuffs in Norway and recommended internationally. Given the highly conservative nature of this assessment and the undoubted highly pessimistic prognosis regarding the contamination of food-chains, the potential requirement for restrictions on the consumption of seafood can be essentially dismissed. The annual effective doses to individuals representing critical groups from the Kola Peninsula and a high rate seafood consumer in Norway were estimated as 11 – 13 µSv and 31 – 39 µSv respectively, values which may be considered to be low when compared to the radiation dose to the average Norwegian from food and drinking water which has been estimated to be 0.52 mSv/year from naturally occurring sources.

The maximum total terrestrial deposition to Norway for all atmospheric model runs resulted in a ^{137}Cs and ^{90}Sr deposition of 97 and 79 TBq, respectively. Considering all relevant exposure pathways, the estimated annual effective dose to individuals in the identified population group in Norway based on releases to atmosphere from a hypothetical accident during transport from Andreeva Bay was of the order of 21 mSv, the main component arising from ingestion of food should no interventions be applied. In the event of a real accident with releases at the worst case hypothesized levels, food interventions levels would be exceeded, and critical groups would be controlled from ingesting highly contaminated foodstuffs. As internal doses from terrestrial food products are almost three orders of magnitude greater than the internal doses for a high rate fish consumer living in Norway, it is clear that the predominant risk to Norwegian populations for an accident involving the transport of SNF from Andreeva to Murmansk would be via an atmospheric transport pathways and terrestrial food-chains.

Regarding dose rates to biota from a hypothetical marine release, the highest dose-rates for the modelled scenarios are observed for the benthic group, with crustaceans and molluscs exhibiting dose rates often exceeding 0.1 µGy/h over the course of the simulation and, in the most extreme case, attaining exposure levels exceeding 0.25 µGy/h for a short period in the case of the circulation pattern from 2010. The levels of exposure of pelagic organisms are substantially lower, by contrast, and only slightly exceed 0.05 µGy/h for a short period of time in the case of seabirds and the circulation patterns for 1998 and 2010. Dose rates for other pelagic organisms are relatively low for all circulation patterns, with fish exhibiting exposures substantially below 0.01 µGy/h.

It should be noted that estimates detailed in the report are derived for conservative, worst-case scenarios for which the probability of occurrence can be considered as very low.

5 References

Åhman B (2007). Modelling radiocaesium transfer and long-term changes in reindeer. Journal of Environmental Radioactivity 2007; 98(1-2): 153-165.

Aarkrog, A., Baxter, M.S., Bettencourt, A.O., Bojanowski, R., Bologa, A., Charmasson, S., Cunha, I., Delfanti, R., Duran, E., Holm, E., Jeffree, Livingston, H.D., Mahapanyawong, S., Nies, H., Osvath, I., Pingyu, Li, Povinec, P.P., Sanchez, A., Smith, J.N. and Swift, D. (1997). A comparison of doses from 137Cs and 210Po in marine food: a major international study. J. Environ. Radioact., 34(1): 69-90.

AMAP (1998). AMAP assessment report: Arctic pollution issues. Oslo: Arctic Monitoring and assessment programme (AMAP), 1998.

Andersson, K.G., Nielsen, S.P., Thørring, H. et al. (2011). Revision of deposition and weathering parameters for the ingestion dose module (ECOSYS) of the ARGOS and RODOS decision support systems. Journal of Environmental Radioactivity 2011; 102(11): 1024-1031.

Antipov S.V., Bilashenko V.P., Vysotskii V.L., Kalantarov V.E., Kobrinskii M.N., Sarkisov A.A. et al. (2015). Prediction and evaluation of the radioecological consequences of a hypothetical accident on the sunken nuclear submarine B-159 in the Barents Sea. Atomic Energy 2015: 119(2): 132-141.

Avila R., Broed R., Pereira A. (2005) ECOLEGO - A toolbox for radioecological risk assessment. In: Proceedings of the International Conference on the Protection from the Effects of Ionizing Radiation, Stockholm (Sweden) 6.-10. October 2003. IAEA-CN-109/80. Vienna: International Atomic Energy Agency, 2003: 229-232.

Bartnicki J., Haakenstad H., Hov Ø. 2011. Operational SNAP model for remote applications from NRPA. Met report 12. Oslo: Norwegian Meteorological Institute, 2011.

Beresford, N.A., Barnett, C.L., Jones, D.G., Wood, M.D., Appelton, J.D., Breward, N. et al (2008a). Background exposure rates of terrestrial wildlife in England and Wales. Journal of Environmental Radioactivity 2008; 99(9): 1430–1439.

Beresford, N.A., Barnett, C.L., Howard, B.J., Scott, W.A., Brown, J.E., Copplestone, D. (2008b). Derivation of transfer parameters for use within the ERICA Tool and the default concentration ratios for terrestrial biota. Journal of Environmental Radioactivity 2008; 99(9): 1393-1407.

Beresford, N.A., Barnett, C.L., Brown, J.E., Cheng, J.J., Copplestone, D., Gaschak, S. et al. (2010). Predicting the radiation exposure of terrestrial wildlife in the Chernobyl exclusion zone: an international comparison of approaches. Journal of Radiological Protection 2010; 30(2): 341–373.

Beresford, N.A., Beaugelin-Seiller, K., Burgos, J., Cujic, M., Fesenko, S., Kryshev, A., Pachal, N.,Real, A., Su, B.S., Tagami, K., Vives i Batlle, J., Vives-Lynch, S., Wells, C., Wood, M.D. (2015). Radionuclide biological half-life values for terrestrial and aquatic wildlife. Journal of Environmental Radioactivity, 150, pp. 270-276.

Boroughs, H., Townsley, S.J., Hiatt, R.W. (1956). The metabolism of radionuclides by marine organisms. I. The uptake, accumulation and loss of strontium89 by fishes. The Biological Bulletin, 111 (no. 3), pp. 336-351.

Brown, J., Strand P., Hosseini, A., Børretzen, P. (2003). Handbook for assessment of the exposure of biota to ionising radiation from radionuclides in the environment. FASSET deliverable 5. https://wiki.ceh.ac.uk/display/rpemain/FASSET+reports (09.11.2017)

Brown JE, Jones SR, Saxén R et al (2004a). Radiation doses to aquatic organisms from natural radionuclides. Journal of Radiological Protection 2004; 24(4A): A63-A77.

Brown, J., Børretzen, P., Dowdall, M., Sazykina, T., Kryshev, I. (2004b). The derivation of transfer parameters in the assessment of radiological impacts to Arctic marine biota. Arctic; 57(3): 279-289.

Brown JE, Alfonso B, Avila R, Beresford NA, Copplestone D, Pröhl G et al (2008). The ERICA tool. Journal of Environmental Radioactivity 2008; 99(9): 1371-1383.

Brown, J. , Hosseini, A. , Karcher, M. , Kauker, F. , Dowdall, M. , Schnur, R. and Strand, P. (2016a): Derivation of risk indices and analysis of variablility for the management of incidents involving the transport of nuclear materials in the Northern Seas , Journal of Environmental Management, 171 , pp. 195-203 . doi: 10.1016/j.jenvman.2016.02.012

Brown, J., Amundsen, I., Bartnicki, J., Dowdall, M., Dyve, J.E., Hosseini, A., Klein, H., Standring, W., (2016b). Impacts on the terrestrial environment in case of a hypothetical accident involving the recovery of the dumped Russian submarine K-27. J. Environ. Radioact. 165, 1-12.

Brown JE, Alfonso B, Avila R, Beresford NA, Copplestone D, Hosseini A (2016c). A new version of the ERICA tool to facilitate impact assessments of radioactivity on wild plants and animals. Journal of Environmental Radioactivity 2016; 153: 141-148.

Buesseler, K.O. (2012). Fishing for answers off Fukushima. Science 2012; 338(6106): 480-482.

Børretzen, P., Salbu, B. (2009). Bioavailability of sediment-associated and low molecular-mass species of radionuclides/trace metals to the mussel Mytilus edulis. Journal of Environmental Radioactivity 2009; 100(4): 333–341.

Coughtrey, P.J., Thorne, M.C. (1983). Radionuclide distribution and transport in terrestrial and aquatic ecosystems: a critical review of data. Volume 1. Rotterdam: A.A. Balkema, 1983.

EFSA (European Food Safety Authority) (2011). Use of the EFSA comprehensive European food consumption database in exposure assessment. EFSA Journal 2011; 9(3): 2097.

Eriksen, E., H. Gjøsæter, D. Prozorkevich, E. Shamray, A. Dolgov, M. Skern-Mauritzen, J.E. Stiansen, Yu. Kovalev, K. Sunnanå (2017): From single species surveys towards monitoring of the Barents Sea ecosystem, Progress in Oceanography, 2017, ISSN 0079-6611, https://doi.org/10.1016/j.pocean.2017.09.007.

Fesenko, S., Sanzharov,a N., Tagami, K. (2009). Evolution of plant contamination with time. In: Quantification of radionuclide transfer in terrestrial and freshwater environments for radiological assessments. IAEA-TECDOC 1616. Vienna: International Atomic Energy Agency (IAEA), 2009: 259263.

Finstad, G.L., Prichard, A.K. (2000). Growth and body weight of free-range reindeer in western Alaska. Rangifer 2000; 20(4): 221-227.

Fisher, N.S. (2002). Advantages and problems in the application of radiotracers for determining bioaccumulation of contaminants in aquatic organisms. In: Børretzen P, Jølle T, Strand P (eds). Proceedings of the International conference on radioactivity in the environment, Monaco 1–5 September 2002. Østerås: Norwegian Radiation Protection Authority, 2002: 573–576.

Gerdes R., Karcher M., Kauker F. and Koeberle C. (2001): Prediction for the spreading of radioactive substances from the sunken submarine "Kursk" in the Barents Sea. EOS transactions, AGU, Vol. 82, No. 23, pp. 253, 256-257.

Gerdes, R., Hurka, J., Karcher, M., Kauker, F., Koeberle, C. (2005). Simulated history of convection in the Greenland and Labrador seas 1948-2001, AGU monograph Climate Variability of the Nordic Seas, Bjerknes Centre for Climate Research, Bergen, Norway, 221-238.

Golikov, V., Logacheva, I., Bruk, G., Shutov, V., Balonov, M., Strand, P. et a.l (2004). Modelling of long-term behaviour of caesium and strontium radionuclides in the Arctic environment and human exposure. Journal of Environmental Radioactivity 2004; 74(1-3): 159–169.

Gómez-Ros, J-M, Pröhl, G., Ulanovsky, A., Lis, M. (2008). Uncertainties of internal dose assessment for animals and plants due to non-homogeneously distributed radionuclides. Journal of Environmental Radioactivity 2008; 99(9): 1449-1455.

Gwynn JP, Brown J, Kovacs KM, Lydersen G (2006). The derivation of radionuclide transfer parameters for and dose-rates to an adult ringed seal (Phoca hispida) in an Arctic environment. Journal of Environmental Radioactivity 2006; 90(3): 197-209.

Gwynn, J.P., Heldal, H.E., Gäfvert, T., et al. (2012). Radiological status of the marine environment in the Barents Sea. Journal of Environmental Radioactivity, 2012; 113: 155–162.

Harms, I., Karcher, M. (2005). Kara Sea freshwater dispersion and export in the late 1990s, Journal of geophysical research-oceans, 110, C08007. doi:10.1029/2004JC002744.

Heldal H. E., Brungot A-L., Skjerdal H., Gäfvert T., Gwynn J. P., Sværen I., Liebig P. L., Rudjord A-L. (2015). Radioaktiv forurensning i fisk og sjømat i perioden 1991-2011 StrålevernRapport 2015:17. Østerås: Statens strålevern, 2015.

Henriksen, T., Saxebøl, G. (1988). Fallout and radiation doses in Norway after the Chernobyl accident. Environment International, 1988, 14/2: , 157-163,

Hibler W.D. III (1979): A dynamic thermodynamic sea ice model. Journal of Physical Oceanography, 1979, Vol. 9, pp 815-846.

Holloway G. Dupont F. Golubeva E. et al. (2007). Water properties and circulation in Arctic Ocean models. JOURNAL OF GEOPHYSICAL RESEARCH, VOL. 112, C04S03, doi: 10.1029/2006JC003642.

Hosseini, A., Amundsen, I., Bartnicki, J., Brown, J., Dowdall, M., Dyve, J.E., Harm, I., Karcher, M., Kauker, F., Klein, H., Lind, O.C., Salbu, B., Schnur, R., Standring, W. (2016). Environmental modelling and radiological impact assessment associated with hypothetical accident scenarios for the nuclear submarine K-27. StrålevernRapport 2016:8 Østerås: Statens strålevern, 2016.

Hosseini, A., Amundsen, I., Brown, J.E., Dowdall, M., Dyve, J.E., Klein H. (2017). Radiological impact assessment for hypothetical accident scenarios involving the Russian nuclear submarine K-159. StrålevernRapport 2017:12. Østerås: Statens strålevern, 2017.

IAEA (1996). Modelling of radionuclide interception and loss processes in vegetation and of transfer in semi-natural ecosystems: second report of the VAMP terrestrial working group. IAEA-TECDOC857. Vienna: International Atomic Energy Agency, 1996.

IAEA (1998). Radiological conditions of the Western Kara Sea: assessment of the radiological impact of the dumping of radioactive waste in the Arctic Seas. Radiological assessment reports series 4. Vienna: IAEA, 1998.

IAEA (1999). Inventory of radioactive waste disposals at sea. IAEA-TECDOC-1105. Vienna: International Atomic Energy Agency, 1999.

IAEA (2003). Determining the suitability of materials for disposal at sea under the London Convention 1972: a radiological assessment procedure. IAEA-TECDOC-1375. Vienna: IAEA, 2003.

IAEA (2004). Sediment distribution coefficients and concentration factors for biota in the marine environment. Technical reports series 422. Vienna: International Atomic Energy Agency, 2004.

IAEA (2009). Quantification of radionuclide transfer in terrestrial and freshwater environments for radiological assessments. IAEA-TECDOC-1616. Vienna: International Atomic Energy Agency, 2009.

IAEA (2010). Handbook of parameter values for the prediction of radionuclide transfer in terrestrial and freshwater environments. IAEA technical report series 472. Vienna: International Atomic Energy Agency, 2010.

IAEA (2014). Handbook of parameter values for the prediction of radionuclide transfer to wildlife. IAEA technical report series 479. Vienna: International Atomic Energy Agency, 2014.

IAEA (2015). Determining the suitability of materials for disposal at sea under the London Convention 1972 and London Protocol 1996: a radiological assessment procedure. IAEA-TECDOC1759. Vienna: International Atomic Energy Agency, 2014.

ICRP (1979). Limits for intakes of radionuclides by workers. ICRP publication 30 (Part 1). Annals of the ICRP 1979; 2(3-4).

ICRP (1995a). Age-dependent doses to members of the public from intake of radionuclides - part 3 ingestion dose coefficients. ICRP publication 69. Annals of the ICRP 1995; 25(1).

ICRP (1995b). Age-dependent doses to members of the public from intake of radionuclides - part 4 inhalation dose coefficients. ICRP publication 71. Annals of the ICRP 1995; 25(3-4).

ICRP (2007). The 2007 recommendations of the International Commission on Radiological Protection. ICRP publication 103. Annals of the ICRP 2007; 37(2-4).

ICRP (2008). Environmental protection: the concept and use of reference animals and plants. ICRP publication 108. Annals of the ICRP 2008; 38(4-6).

ICRP (2009). Environmental protection: transfer parameters for reference animals and plants. ICRP publication 114. Annals of the ICRP 2009; 39(6).

ICRP (2014). Protection of the environment under different exposure situations. ICRP publication 124. Annals of the ICRP 2014; 43(1).

Kagan, B.A., E.V. Sofina, (2015): published in Izvestiya AN. Fizika Atmosfery i Okeana, 2015, Vol. 51, No. 6, pp. 729–740.DOI: 10.1134/S0001433815060079.

Kalnay E, Kanamitsu M, Kistler R et al. (1996). The NCEP/NCAR 40-year reanalysis project, B. Am. Meteorol. Soc., 77, 437–471.

Karcher, M. J., Gerdes, R., Kauker, F., Koeberle, C. (2003). Arctic warming - Evolution and Spreading of the 1990s warm event in the Nordic Seas and the Arctic Ocean, Journal of Geophysical Research, Vol. 108(C2), 3034. doi:10.1029/2001JC001265

Karcher, M., A. Hosseini, R. Schnur, F. Kauker, J.E. Brown, M. Dowdall, P. Strand (2017): Modelling dispersal of radioactive contaminants in Arctic waters as a result of potential recovery operations on the dumped submarine K-27, Marine Pollution Bulletin, Volume 116, Issues 1–2, 2017, Pages 385-394, ISSN 0025-326X, doi.org/10.1016/j.marpolbul.2017.01.034.

Karcher, M., Gerdes, R., Kauker, F. (2008). Long-term variability of Atlantic water inflow to the Northern Seas: insights from model experiments, Arctic-Subarctic Ocean Fluxes: Defining the role of the Northern Seas in Climate, Editors: B. Dickson, J. Meincke and P. Rhines, Springer.

Karcher, M., Smith, J. N., Kauker, F., Gerdes, R., & Smethie, W. M. (2012). Recent changes in Arctic Ocean circulation revealed by iodine-129 observations and modeling. Journal of Geophysical Research: Oceans (1978–2012), 117(C8).

Karcher, M.J., Kulakov, M., Pivovarov, S., Schauer, U., Kauker, F., Schlitzer, R. (2003): Atlantic Water flow to the Kara Sea - comparing model results with observations, in: 'Siberian River Runoff in the Kara Sea: Characterisation, Quantification, Variability and Environmental Significance', Stein, Fahl, Fütterer, Galimov (Eds.), Elsevier, Proceedings in Marine Science, 47-69.

Karcher, M.J., S. Gerland, I. H. Harms, M. Iosjpe, H. E. Heldal, P. J. Kershaw and Sickel, M. (2004): The dispersion of ^{99}Tc in the Nordic Seas and the Arctic Ocean: a comparison of model results and observations, Journal of environmental radioactivity, Vol.74, 1-3, 2004, pp. 185-198.

Kauker, F. , Kaminski, T. , Karcher, M. , Dowdall, M. , Brown, J. , Hosseini, A. and Strand, P. (2016): Model analysis of worst place scenarios for nuclear accidents in the northern marine environment , Environmental Modelling & Software, 77 , pp. 13-18 . doi: 10.1016/j.envsoft.2015.11.021

Karlsen, S.R., Elvebakk, A., Høgda, K.A., Johansen, B. (2006). Satellite based mapping of the growing season and bioclimatic zones in Fennoscandia. Global Ecology and Biogeography 2006; 15(4): 416– 430.

Kato H, Onda Y, Teramage M (2012). Depth distribution of ^{137}Cs, ^{134}Cs, and ^{131}I in soil profile after Fukushima Dai-ichi nuclear power plant accident. Journal of Environmental Radioactivity 2012; 111: 59-64.

Kauker, F., Gerdes, R., Karcher, M., Koeberle, C., Lieser, J.L. (2003): Variability of Arctic and North Atlantic sea ice: A combined analysis of model results and observations from 1978 to 2001, Journal of Geophysical Research, 108(C6), 3182. doi:10.1029/2002JC001573.

Kirchner, G., Daillant, O. (2002). The potential of lichens as long-term biomonitors of natural and artificial radionuclides. Environmental Pollution 2002; 120(1): 145–150.

Komperød M, Rudjord AL, Skuterud L et al (2015). Radiation doses from the environment. Calculations of the public's exposure to radiation from the environment in Norway. StrålevernRapport 2015:11. Østerås: Norwegian Radiation Protection Authority, 2015.

Köberle, C. and Gerdes, R. (2003): Mechanisms determining the variability of Arctic sea ice conditions and export, Journal of Climate, 16, pp. 2843-2858

Landrum, P.F., Lydy, H.L., Lee, H. (1992). Toxicokinetics in aquatic systems: model comparison and use in hazard assessment. Environmental Toxicology and Chemistry 1992; 11(12): 1709–1725.

Larsson CM (2008). An overview of the ERICA Integrated Approach to the assessment and management of environmental risks from ionising contaminants. Journal of Environmental Radioactivity 2008; 99(9): 1364-1370.

Liland, A., Lochard, J., Skuterud, L. (2009). How long is long-term? Reflections based on over 20 years of post-Chernobyl management in Norway. Journal of Environmental Radioactivity 2009; 100(7): 581584.

Loeng, H. (1991) Features of the physical oceanographic conditions of the Barents Sea, Polar Research, 10:1, 5-18, DOI: 10.3402/polar.v10i1.6723

Mitchell, N.G. (2001). Models for radionuclide transfer to fruits and data requirements. Journal of Environmental Radioactivity 2001; 52(2-3): 291-307.

Nagy KA (2001). Food requirements of wild animals: predictive equations for free-living mammals, reptiles, and birds. Nutrition Abstracts and Reviews Series B, Livestock Feeds and Feeding 2001; 71(10): 21R–32R

Nordic Flagbook, 2014. Protective Measures in Early and Intermediate Phases of a Nuclear or Radiological Emergency: Nordic Guidelines And Recommendations. Joint report of the Nordic Radiation Protection Authorities: www.stralsakerhetsmyndigheten.se/Global/Pressmeddelanden/2014/Nordic%20Flagbook%20February%202014.pdf.

NRPA (2011). Radioactivity in the marine environment 2008 and 2009. Results from the Norwegian National Monitoring Programme (RAME). StrålevernRapport 2011:4. Østerås: Norwegian Radiation Protection Authority, 2011.

NRPA (2015). Radioactivity in the Marine Environment 2011. Results from the Norwegian Marine Monitoring Programme (RAME). StrålevernRapport 2015:3. Østerås: Norwegian Radiation Protection Authority, 2015.

Pacanowski, R. C., 1995: MOM2 Documentation, User's Guide, and Reference Manual. NOAA/Geophysical Fluid Dynamics Laboratory.

Reistad M, Breivik Ø, Haakenstad H, Aarnes OJ, Furevik BR, Bidlot J-R (2011). A high resolution hindcast of wind and waves for the North Sea, the Norwegian Sea and the Barents Sea. Journal of Geophysical Research 2011; 116(C5): C05019.

Sazykina, T.G. (1998). Long-distance radionuclide transfer in the Arctic Seas related to fish migrations. Radiation Protection Dosimetry 1998; 75(1-4): 219-222.

Schino, G., Borfecchia, F., De Cecco, L., Dibari, C., Iannetta, M., Martini, S. et al. (2003). Satellite estimate of grass biomass in a mountainous range in central Italy. Agroforestry Systems 2003; 59(2): 157–162.

Shilov, V.V., Lazarev A.L., Krakhmalev, S.Yu., Kolobaev, A.A., Novikov, V.P., Timofeev M.S.,Ivanova, A.S., Ivanova, M.L. Editors: Dowdall, M.J., Standring, W.J.F., Amundsen I.B. Environmental Impact Assessment Of The Removal of Spent Nuclear Fuel (SNF) From Andreeva Bay. StrålevernRapport 2017:9. Østerås: Statens strålevern, 2017.

Skuterud L, Gwynn JP, Gaare E et al (2005). ^{90}Sr, ^{210}Po and ^{210}Pb in lichen and reindeer in Norway. Journal of Environmental Radioactivity 2005; 84(3): 441-456.

Staaland, H., Garmo, T.H., Hove, K., Pedersen, Ø. (1995). Feed selection and radiocaesium intake by reindeer, sheep and goats grazing alpine summer habitats in southern Norway. Journal of Environmental Radioactivity 1995; 29(1): 39-56.

Steele, M., R. Morley, and W. Ermold, 2001: Phc- a global ocean hydrography with a high-quality arctic ocean. J. Climate, 14 (9), 2079–2087.

Stevens D.P., (1991). A numerical ocean circulation model of the Norwegian and Greenland Seas. Progress in Oceanography, Volume 27, Issues 3–4, Pages 365-402.

Tantsiura (1959). About the currents in the Barents Sea, Trudy polyar, naucho-issled. Inst. morsk. ryb. Khoz. Okeanogr., 11, 35-53 (In Russian).

Terziev et al. (1990): Hydrometeorology and Hydrochemistry of USSR Seas, Vol. 1: The Barents Sea, Ed. by F. S. Terziev, G. V. Girdyuk, G. G. Zykova, and S. L. Dzhenyuk (Gidrometeoizdat),

Thomann, R.V. (1981). Equilibrium model of fate of microcontaminants in diverse aquatic foodchains. Canadian Journal of Fisheries and Aquatic Sciences 1981; 38(3): 280-296.

Thørring, H., Ytre-Eide, M.A., Liland, A. (2010). Consequences in Norway after a hypothetical accident at Sellafield: Predicted impacts on the environment. StrålevernRapport 2010:13. Østerås: Statens strålevern, 2010.

Tømmervik H, Johansen B, Riseth JÅ, Karlsen SR, Solberg B, Høgda KA (2009). Above ground biomass changes in the mountain birch forests and mountain heaths of Finnmarksvidda, Northern Norway, in the period 1957–2006. Forest Ecology and Management 2009; 257(1): 244–257.

Uhlig, C., Sveistrup, T.E., Schjelderup, I. (2004). Impacts of reindeer grazing on soil properties on Finnmarksvidda, northern Norway. Rangifer 2004; 24(special issue 15): 83-91.

Ulanovsky, A., Pröhl, G. (2006). A practical method for assessment of dose conversion coefficients for aquatic biota. Radiation and Environmental Biophysics 2006; 45(3): 203-214.

Ulanovsky, A., Pröhl, G., Gómez-Ros, J-M- (2008). Methods for calculating dose conversion coefficients for terrestrial and aquatic biota. Journal of Environmental Radioactivity 2008; 99(9): 1440-1448.

UNSCEAR (1993). Ionizing Radiation: Sources and Biological Effects. United Nations, New York.

UNSCEAR (2008). Sources and effects of ionizing radiation, UNSCEAR 2008 report: Volume II: Annex E: Effects of ionizing radiation on non-human biota. New York: United Nations, 2008.

UNSCEAR (2014). Sources, effects and risks of ionizing radiation, UNSCEAR 2013 report: Volume I: Annex A: Levels and effects of radiation exposure due to the nuclear accident after the 2011 great east-Japan earthquake and tsunami. New York: United Nations, 2014.

USDoE (2002). A graded approach for evaluating radiation doses to aquatic and terrestrial biota. Technical standard DOE-STD-153-2002. Washington, DC: U.S. Department of Energy, 2002.

Vidal, M., Roig, M., Rigol, A., Montserrat, L., Rauret, G., Wauters, J. et al. (1995). Two approaches to the study of radiocaesium partitioning and mobility in agricultural soils form the Chernobyl area. Analyst 1995; 120(6): 1785-1791.

Vives i Batlle, J., Wilson, R.C., Watts, S.J., Jones, S.R., McDonald, P., Vives-Lynch, S. (2008). Dynamic model for the assessment of radiological exposure to marine biota. Journal of Environmental Radioactivity 2008; 99(11): 1711-1730.

Vives i Batlle, J., Beresford, N.A., Beaugelin-Seiller, K., Bezhenar, R., Brown, J., Cheng, J-J. et al. (2016). Intercomparison of dynamic models for radionuclide transfer to marine biota in a Fukushima accident scenario. Journal of Environmental Radioactivity 2016; 153: 31-50.

Wang, W.X., Ke, C.H., Yu, K.N., Lam, P.K.S. (2000). Modelling the bioaccumulation of radiocesium in a marine food chain. Marine Ecology Progress Series 2000; 208:41–50.

Watson, W.S., Sumner, D.J., Baker, J.R., Kennedy, S., Reid, R., Robinson, I. (1999). Radionuclides in seals and porpoises in the coastal waters around the UK. Science of the Total Environment 1999; 234(1-3): 113.

Whicker FW, Schultz V (1982). Kinetics of compartment systems. In: Radioecology: nuclear energy and the environment, volume II. Boca Raton, FL: CRC Press, 1982: 64-117.

Wienerroither R., Johannesen E., Dolgov A., Byrkjedal I., Bjelland O, Drevetnyak K., Eriksen KB., Høines Å., Langhelle G., Langøy H., Prokhorova T., Prozorkevich D., Wenneck T., (2011). Atlas of the Barents Sea fishes. IMR/PINRO joint report series 1-2011. Bergen: Institute of Marine Research, 2011.

6 Appendices

6.1 Appendix A – Modelling transfer of radionuclides in marine food-chains

A model, based on the work of Thomann (1981), Landrum et al. (1992), and Fisher (2002), was used to simulate the uptake of radionuclides via food and water by aquatic organisms and transfer through marine food-chains. Excretion/ elimination rates were assumed to be independent of the uptake route, the assimilation efficiency was assumed to be independent of food type, and predators were assumed not to assimilate the activity concentration in the gut content of their prey. Further assumptions were that the zooplankton were a homogeneous group, described by specified parameter values rather than by ranges, and that the growth rate for all organisms was 0. This last assumption may be a less robust than the others (Thomann, 1981), but the complexity of the weight dynamics for the organisms in question would require further, more detailed study and were anticipated as adding little in terms of yielding more accurate prognoses. The time-dependent transfer of radionuclides to considered marine organisms (mollusks, crustaceans, fish, seal and sea bird) within the food chain can be described by simple, first-order differential equations. This approach was adopted as opposed to using only equilibrium-based concentration ratios because kinetic models are much better suited to simulating transfer through food-chains when seawater concentrations are changing rapidly as in the case of accidental releases (i.e. steady state/equilibrium conditions are not prevalent). An earlier version of the model is described in Brown et al. (2004b) with a condensed explanation provided below. For prey species (i.e. phytoplankton for mollusk; zooplankton for fish, steady state conditions between radionuclide activity concentrations in biota and water are assumed, allowing the application of concentration ratios:

$$C_p = CR_p \cdot C_w \quad \text{(A-1)}$$

Where:

C_p is the radionuclide activity concentration in prey species (Bq kg^{-1} f.w.);

CR_p is the concentration ratio for prey species (l kg^{-1}); and

C_w is the radionuclide activity concentration in sea water (Bq l^{-1}).

For fish, accounting for radionuclide uptake via water and food, the following equation is applied:

$$\frac{dC_f}{dt} = AE_f \cdot IR_f \cdot C_P + k_{uf} \cdot C_w - C_f \cdot k_{ef} \quad \text{(A-2)}$$

Where:

AE_f is the assimilation efficiency (dimensionless) for fish;

IR_f is the ingestion rate per unit mass of fish (kg f.w. d^{-1} per kg f.w.);

k_{uf} is the uptake rate of radionuclide to fish directly from water column (l/kg d^{-1});

C_f is the activity concentration in fish (Bq kg^{-1} f.w.);

k_{ef} is the depuration rate from fish (d^{-1}).

Similar equations are used for mollusk and for crustaceans but using parameters appropriate for these organism groups. An overview is provided in Table A.1 with the provenance of the data given in each case. Modelling the kinetics of radiocaesium transfer for crustaceans was problematic owing to the large and varied diet of this organism group. For the purposes of this work, this category of biota was assumed to be a large crustacean preying on mussels and scavenging on the remains of pelagic organisms. The consistency of prey species has been crudely assumed to be formed from 50 % mollusk and 50 % fish. In practice, this means that the input values of C_p for the crustacean model have been derived from the output of the fish and mollusk models.

One way to consider radionuclide transfer to seals, based on the work of Brown et al. (2004b), is through Eq. A-3.

$$\frac{dC_s}{dt} = \sum_{1}^{n} (x_i . AE_s \cdot IR_s \cdot C_i) - C_s \cdot k_{es} \qquad \text{(A-3)}$$

Where:

x_i is the fraction of the diet associated with dietary component “i”

AE_s,i is the assimilation efficiency (dimensionless) for dietary component “i”

IR_s is the ingestion rate per unit mass of seal (kg f.w. d^{-1} per kg f.w.)

C_i is the activity concentration in the dietary component “i” (Bq kg^{-1} f.w.)

Cs is the “whole body” activity concentration in the seal (Bq kg^{-1} f.w.)

k_{es} is the effective loss rate from seal (d^{-1}) – incorporating both excretion rate and physical decay of the radionuclide

A similar approach can be adopted to model the time varying activity concentrations in seabirds, C_b, with a requirement to then provide specific values for the parameters IR_b (the ingestion rate per unit mass for seabirds), AE_b (the assimilation efficiency of radiocaesium for seabirds) and k_{eb} (the effective loss rate of radiocaesium for seabirds).

An ingestion rate, IR_s, of 0.072 kg f.w. day^{-1} per kg f.w. seal was derived by Gwynn et al. (2006) using allometric relationships (Nagy, 2001) for carnivora (Eq. A-4)

$$FMI = 0.348M^{0.859} \qquad \text{(A-4)}$$

where FMI is the fresh matter intake (g/day) and M is the mass of the seal (g).

In a similar way, Nagy (2001) provides the allometric relationship for marine birds (Eq. A-5):

$$FMI = 3.221M^{0.658} \qquad \text{(A-5)}$$

where FMI is the fresh matter intake (g/day) and M is the mass of the bird (g).

A representative mass of 1.26 kg, commensurate with the value used for marine birds in the ERICA Tool (Brown et al., 2008), was used as a default for calculations. This yields an IR_b of 0.28 kg f.w. day^{-1} per kg f.w. seabird.

For seals and sea birds, the assimilation efficiencies for ^{137}Cs were set to unity commensurate with generic values that are normally applied for mammals (Brown et al., 2003). For the sake of simplicity, it was also assumed that the seals and seabirds live entirely off fish. The term x_i =1 in Eq. A-3 and C_i is equal to the (time varying) activity concentration in fish derived using the approach outlined earlier. Harp seals, for example, have a varied diet of fish including species such as capelin, polar and Arctic cod and herring. Although they also are known to consume crustaceans, the simplification of the diet was not considered to be unduly problematic. Since a generic group was also being considered in the case of seabirds, similar contentions are valid – assuming the entire diet is based on fish would appear to be a reasonable assumption.

A whole-body biological half-life of 29 days was derived by Gwynn et al. (2006) for ^{137}Cs in an adult ringed seal. This compares to values for grey and harbour seals of 20 days from the Baltic Sea (Holm et al., 2005) and 28 days from the UK and Ireland (Watson et al., 1999). A value of 29 days was adopted in this work as a conservative approximation, i.e. the longer the retention time of a given radionuclide for a specified intake the greater will be the concomitant internal exposure. Deriving biological half-lives for sea birds is a more uncertain process in which recourse was made to the allometric relationships for biological loss provided by Whicker & Shultz (1982) for caesium. The following formula can be applied.

$$k_a = \frac{\ln 2}{18.36 M^{0.24}} \qquad \text{(A-6)}$$

where k_a = the effective loss rate for the animal (d^{-1}), M = mass of animal (kg, f.w.).

This gave a k_b of 0.036 d^{-1} corresponding to a biological half-life of radiocaesium in birds of ca. 19 days. This value, as used in Hosseini et al. (2017), appears to be a little on the high side (in view of information concerning other organism groups) but was likely to provide a conservative estimate of transfer in keeping with accepted approaches to err on the side of caution when model parameters are considered to be uncertain. An overview of all of the parameters used in the (bio-) kinetic models is presented in Table A.1 (for ^{137}Cs) and Table A.2 (for ^{90}Sr).

Table A.1: Parameters used in the kinetic model for ^{137}Cs in the marine environment (from Hosseini et al. (2017))

Parameter	Organism Modelled	Value (units)	Reference/comment
CR_p	Fish	130	IAEA (2014); Arithmetic mean value for zooplankton
CR_p	Mollusc	8.5	IAEA (2014); Arithmetic mean value for phytoplankton
AE_f	Fish	0.5 (dimensionless)	Brown et al. (2004b)
AE_M	Mollusc	0.5 (dimensionless)	Vive I Batlle et al. (2016); Value form BURN-P model
AE_C	Crustacean	0.5 (dimensionless)	Vives I Batlle et al. (2016); Value from BURN-P model
AE_s	Seal	1 (dimensionless)	Gwynn et al. (2006)
AE_b	(Sea)Bird	1 (dimensionless)	Assumed to be equal to seal
k_{uf}	Fish	0.01 (l/kg d^{-1})	Brown et al. (2004b)
k_{uM}	Mollusc	1.1 mL g^{-1} (dry) h^{-1} = 26.4d^{-1} = 4.75 (l/kg d^{-1})	Børretzen & Salbu (2009)
k_{uC}	Crustacean	0.49 (l/kg d^{-1})	Brown et al. (2004b) for zooplankton
IR_f	Fish	0.009 (kg f.w. d^{-1} per kg f.w.)	Brown et al. (2004b)/Large fish
IR_M	Mollusc	0.2 (kg d^{-1} per kg)	Wang et al. (2000) as applied to Mussel (*Perna viridis*)
IR_C	Crustacean	0.027 (kg f.w. d^{-1} per kg f.w.)	Vives I Batlle et al. (2016); Value from K-BIOTA
IR_s	Seal	0.072 (kg f.w. d^{-1} per kg f.w.)	Gwynn et al. (2006)
IR_b	(Sea)Bird	0.28 (kg f.w. d^{-1} per kg f.w.)	Hosseini et al. (2017) - Derived allometrically – see main text
k_{ef}	Fish	0.0107 (d^{-1})	ICRP (2009)
k_{eM}	Mollusc	0.04 (d^{-1})	Vives I Batlle et al. (2016); Value derived from D-DAT biological half-life
k_{eC}	Crustacean	0.023 (d^{-1})*	Beresford et al. (2015)
k_{es}	Seal	0.0239 (d^{-1})	Gwynn et al. (2006) - Derived allometrically – see main text
k_{eb}	(Sea)Bird	0.036 (d^{-1})	Hosseini et al. (2017) Derived allometrically – see main text

Table A.2: Parameters used in the kinetic model for ^{90}Sr in the marine environment

Parameter	Organism Modelled	Value (units)	Reference/comment
CR_p	Fish	68	IAEA (2014); Arithmetic mean value for zooplankton
CR_p	Mollusc	96	IAEA (2014); Geometric mean value for zooplankton
AE_f	Fish	0.3 (dimensionless)	Values from NRPA model as reported Vives i Batlle et al. (2016)
AE_M	Mollusc	0.28 (dimensionless)	Values from K-Biota model as reported inVives i Batlle et al. (2016)
AE_C	Crustacean	0.33 (dimensionless)	Values from K-Biota model as reported inVives i Batlle et al. (2016)
AE_s	Seal	0.3 (dimensionless)	Values from FASSET D5 (Brown et al., 2003)
AE_b	(Sea)Bird	0.3 (dimensionless)	Values from FASSET D5 (Brown et al., 2003)
k_{uf}	Fish	0.27 (l/kg d^{-1})	Sr-90 derived (approximately) from Boroughs et al. (1956).
k_{uM}	Mollusc	0 (l/kg d^{-1})	No data found so value set to zero (assumed all intake occurs via food - reasonable assumption considering molluscs are filter feeders ?)
k_{uC}	Crustacean	0.27 (l/kg d^{-1})	Sr-90 - values for fish used
IR_f	Fish	0.009 (kg f.w. d^{-1} per kg f.w.)	Brown et al. (2004b)/Large fish
IR_M	Mollusc	0.2 (kg d^{-1} per kg)	Wang et al. (2000) as applied to Mussel (*Perna viridis*)
IR_C	Crustacean	0.027 (kg f.w. d^{-1} per kg f.w.)	Vives I Batlle et al. (2016); Value from K-BIOTA
IR_s	Seal	0.072 (kg f.w. d^{-1} per kg f.w.)	Gwynn et al. (2006)
IR_b	(Sea)Bird	0.28 (kg f.w. d^{-1} per kg f.w.)	Hosseini et al. (2017) - Derived allometrically – see main text
k_{ef}	Fish	0.00495 (d^{-1})	Sr-90 value from Vives i batlle (2016) for D-DAT model - 140 day T0.5biol
k_{eM}	Mollusc	0.022 (d^{-1})	Vives I Batlle et al. (2016); Value derived from D-DAT biological half-life
k_{eC}	Crustacean	0.022 (d^{-1})	Vives I Batlle et al. (2016); Value derived from IRSN biological half-life (32 d)
k_{es}	Seal	0.00586 (d^{-1})	Sr-90 average from all mammals (includes terrestrial) based on long
k_{eb}	(Sea)Bird	0.00586 (d^{-1})	Same as loss rate for mammal (allometric value seemed too low -

6.2 Appendix B – Modelling transfer of radionuclides in terrestrial food chains

A terrestrial food-chain model was used to provide input for both the derivation of ingestion doses for humans and for the assessment of doses to wild plants and animals. In view of available data, it was most appropriate to split the modeling into flora (Wild grass/grasses, herbs and shrub) and fauna (Deer/herbivorous mammal and rat/burrowing mammal) partly based on the classifications given in UNSCEAR (2008).

Using a variant of the methodology given in UNSCEAR (2008, 2014), the activity concentration in flora can be derived from the total deposition using an expression accounting for interception by foliage, direct deposition onto soil, weathering losses of radionuclides from vegetation and uptake from soil to plant.

In case of an acute deposition the radionuclide content on vegetation at time 't', accumulated via direct deposition from the air, can be calculated (as outlined in Brown et al., 2003) as:

$$C^{air}_{flora,r} = \frac{f_{flora} \cdot D_{tot,r}}{b_{flora}} \cdot [e^{(-(\lambda_{flw,r}+\lambda_r)\cdot t)}] \quad \text{(B-1)}$$

where

$C_{flora,r}$ is the radionuclide activity concentration in flora from air deposition (Bq kg^{-1} f.w.)

f_{flora} is the interception fraction for a given flora (dimensionless)

$D_{tot,r}$ is the total deposition of radionuclide 'r' (Bq m^{-2})

$_{flw,r}$ is the weathering constant for a given flora for radionuclide r(d^{-1})

$_r$ is the decay constant for radionuclide r (d^{-1})

b is standing biomass of the flora (kg m^{-2})

t is time (d)

For the same acute deposition, at time 't', there is also a component of contamination that arises from soil to plant transfer. In this case an assumption is made that for this fraction of the contamination in the plant attributable to root uptake, equilibrium exists between the activity concentration in the plant and the soil.

$$C^{soil}_{flora,r} = \left[\frac{D_{tot,r} \cdot \left[(1 - f_{flora}) + f_{flora} \cdot (1 - e^{-\lambda_{flw,r}t}) \right] \cdot e^{-\lambda_r t}}{\rho_{soil} \cdot d_{soil}} \right] . CR_{flora,r} \quad \text{(B-2)}$$

where

$_{soil}$ is the dry soil density (kg m^{-3} d.m.)d_{soil} is the depth of soil within which radionuclide r has become mixed (m) $CR_{flora,r}$ is the soil to plant concentration ratio for radionuclide r (dimensionless)

All other parameters have been described above in equation (B-1). Application of this model also allows for time varying deposition rates to be considered. For this more complex situation, the problem can be solved numerically.

There is an assumption in this model that a representative interception fraction 'f' for a given flora type can be applied for the entire simulation period. Data compilations for agricultural systems in relation to

this parameter (IAEA, 2010) indicate that the interception fraction depends on whether dry or wet deposition is occurring, the stage of development of the plant and plant type in question, the capacity of the canopy to retain water, elemental properties of the radionuclide, and other factors such as amount and intensity of rainfall in the case of wet deposition and particle sizes of the deposited material. The approach taken here was, therefore, arguably simplistic but in view of the numerous uncertainties involved should at least provide an indication of contamination levels in food-chains following deposition of contamination and at least constitutes an attempt to model the dynamics of interception and loss from flora in contrast to approaches considering soil to plant transfer only. In addition to the interception fraction, biomass, which clearly relates to the stage of development of the plant, also requires further consideration as an important model parameter.

Tømmervik et al. (2009) reported a biomass of 4.13 tonnes/hectare for a 'Field layer' (forbs and grasses) in Northern Finland. This understory biomass would appear to be fairly typical for many other categories of shrub, field, bottom (moss and lichen) layers in mountain birch forests and mountain heaths in this region: Tømmervik et al. (2009) report 1.5 to 5.35 tonnes/hectare for such categories from northern Fenno-scandinavia, including Finnmark). A biomass of 4 tonnes/hectare corresponds to 400 g/m^2. Although Schino et al. (2003) studied grasslands in mountainous areas of central Italy, the work provides an indication of variations in grass biomass that can arise from seasonality and the presence of different species. The recorded range of grass biomass in this aforementioned study was approximately 60 to almost 700 g m^{-2} providing a useful context for our selection of an appropriate biomass value for 'Wild grass/grasses' and for shrubs.

The start and end of the growing seasons (based on data for the period 1982–2002) in the Artic/Alpine and Northern boreal zones to which large areas of Finnmark belong, are June 4-20th and 21-24th September respectively (Karlsen et al., 2006) with a peak in growth occurring towards the end of July/beginning of August. The period selected for the hypothetical release from K-27 was August and September, coinciding with the period where any salvage activity is likely to take place from practical considerations. The deposition would thus occur in the middle of the growing season but following peak growth removing the requirement to model the effect of growth dilution on radionuclide levels. Modelling of this phenomenon would be required were determinations needed for the period coinciding with rapid vegetation biomass increases early in the growing season.

The interception fraction, f, for Cs and grass varies from 0.84 (dry deposition) to 0.027 (wet deposition heavy rain) (IAEA, 2010). A default of 0.43 has been selected for this analysis simply based on the value falling midpoint between the maximum and minimum values reported above. This yields a mass interception fraction f_B of 1.1 (m^2 kg^{-1}) a value which was considered as being typical for Cs deposited on grass following the Chernobyl accident (IAEA, 2010). Owing to the lack of specific information on shrubs, the same default values as grass have been used. As noted by Tømmervik et al. (2009), the shrub layer has a biomass of a similar order of magnitude to the field layer in mid growing season. Although leaf area and surface roughness etc. might be expected to be different between grasses and shrubs the similarity purely in terms of above ground mass available to intercept contaminants render the assumption of similar mass interception fractions a reasonable one. The differences in interception between different elements reflect their different valencies. Plant surfaces are negatively charged and thus may be considered as analogous to a cation exchanger (IAEA, 2009). Therefore, the initial retention of anions such as iodide is less than for polyvalent cations, which seem to be very effectively retained on plant surface. For analyses of data for Chernobyl deposition in Germany, the mass interception factors increase in the order ^{106}Ru, ^{131}I, ^{137}Cs, ^{140}Ba, with these radionuclides having been deposited during the same rainfall event (IAEA, 2009). The highest values were observed for ^{140}Ba, which behaves similarly to strontium. Barium is a bivalent cation and seems to be more strongly retained on the negatively charged plant surface than the monovalent caesium cation.

A mass interception of 1.4 and 0.7 (m^2 kg^{-1}) for ^{137}Cs and ^{90}Sr has been used by Golikov et al. (2004) in modelling the interception by lichen and subsequent transfer of these radionuclides through Arctic foodchains. Aside from the apparent discrepancy with observation for plants – where the magnitude of f_B

is linked with valency – these values constitute a seldom characterization of the apposite process of interception for lichens. Using an assumed lichen biomass of 400 g m^{-2} based loosely on the information of Tømmervik et al. (2009), this information yields interception fractions, of 0.56 and 0.28 for Cs and Sr respectively.

Weathering rates for grass have been derived from the extensive analyses of data undertaken elsewhere (IAEA, 1996). Mitchell (2001) provides an overview of models concerning the transfer radionuclides to fruits. In order to model weathering of radionuclides on plant surfaces, an effective retention half-time was derived for use in the FARMLAND model. A single value of 11 d gave the best fit to experimental data giving a radionuclide independent rate constant of $6.3x10^{-2}$ d^{-1}. The similarity of this value with those applied for grass has led to the application of the same default values for both vegetation categories. Golikov et al. (2004) modelled the loss of Cs-137 and Sr-90 from lichen using short-term and long-term ecological half-lives. For both radionuclides the short-term ecological half-life (1 and 2 years for ^{90}Sr and ^{137}Cs respectively) accounted for losses from the predominant fraction of deposited activity. Longer retention half-lives for Cs-137 in lichen have been reported by Kirchner & Daillant (2002), from their own and other studies, falling between 2.6 to 4.9 years. In view of these data and consideration of the fact that the long-term ecological half-life from Golikov et al. (2004) is ca. 20 years for ^{137}Cs and ^{90}Sr, a default weathering loss rate of 5 years, corresponding to the upper end of the values reported by Kirchner & Daillant (2002), has been applied for both radionuclides in our model.The parameters have been assigned different default values as shown in Table B.1. Two categories of flora –Wild grass/grasses, and shrubs – taken to be representative of berry plants such as *Vaccinium spp*.

The interception of ^{90}Sr has been taken to be a factor of (1.7/1.1 based upon the ratio of ^{140}Ba to ^{137}Cs for Chernobyl from IAEA (2009). According to Andersson et al. (2011), there are no clear differences between the weathering rates for grass that can be attributed to radioceasium and radiostrontium. From this observation the same default value has been used for both radionuclides.

Limitations to the use of concentration ratios[1], CRs, arise from an incompatibility of the application of empirical data based on the long-term post depositional conditions to the period directly following an accident. The CR values used (Table B.2.) are based on empirical datasets from field investigations collated to avoid inclusion of data pertaining to the period directly following depositional events (global fallout and Chernobyl accident deposition for some radionuclides such as Cs, Pu, Sr and Am) and thus should omit values pertaining to surface contamination of vegetation (Beresford et al., 2008b). These default CR data are generally assumed to correspond to, and thus are applicable for, a contaminated soil depth of 10 cm. There is thus an inconsistency with the observed distributions of radionuclides shortly following deposition. Using the Fukushima accident by way of example, Kato et al., (2012) reported that greater than 86% of total radiocaesium and 79% of total ^{131}I were absorbed in the upper 2.0 cm in a soil profile from a relatively contaminated cultivated area sampled, at the end of April 2011, in proximity to (< 50 km distant, in a northeasterly direction) the Fukushima Dai-ichi site. A default value of 5 cm has been used for the calculations undertaken in the current assessment. Furthermore, bioavailability of radiocaesium has been observed to decrease with time following its introduction to soils (Vidal et al., 1995) with the implication that CRs based upon long term post depositional datasets might not reflect the transfer occurring in the early phase depositional environment appropriately. Indeed, this contention is evidenced by reviews of published information on Cs-137 in the soil-plant system shortly after the Chernobyl accident (Fesenko et al., 2009). Finally, soil type, as defined by various soil properties, strongly influences transfer to plants (IAEA, 2010) and there will undoubtedly be differences in the soil types upon which the default data are based and the soil types in Finnmark for which the transfer parameters are applied.

[1] Concentration ratio = activity concentration in whole organism divided by activity concentration in soil

Table B.1. Parameters used in Terrestrial food-chain model.

Parameter	Dependencies : flora, radionuclide	Value	Units and notes	References
$_{soil}$		1550	kg m^{-3} typical soil densities for Finnmarksvidda range between 1.4 and 1.7 g cm^{-3}	Uhlig et al. (2004)
d_{soil}		0.05	m, assumed depth of initial contamination following a deposition event	
f	Wild grass/grasses, Cs	0.43	(Unitless) f varies from 0.84 (dry deposition) to 0.027 (wet deposition heavy rain) (IAEA, 2010)	IAEA, 2010
	Wild	0.66	Bivalent Sr-90 will have a higher f than monovalent Cs (see main text)	IAEA, 2009
f	Shrub, Cs	0.43	As for grass	
	Shrub, Sr	0.66	As for grass	
f	Lichen, Cs	0.56		Golikov et al. (2004)
	Lichen, Sr	0.28		
b	Wild grass/grasses	0.4	kg m^{-2}	Tømmervik et al. (2009)
	Shrub	0.4	kg m^{-2}	
	Lichen	0.4	kg m^{-2}	
$\lambda_{flw,r}$	Wild grass/grasses, Cs	5 x10^{-2}	d^{-1}, Table VIII, p.37 (IAEA, 1996)	IAEA (1996)
	Wild grass/grasses, Sr	5 x10^{-2}	d^{-1}, As for Cs (see main text)	
$\lambda_{flw,r}$	Shrub, Cs	5 x10^{-2}	d^{-1}, As for grass	
	Shrub, Sr	5 x10^{-2}	d^{-1}, As for grass and Cs	
$\lambda_{flw,r}$	Lichen, Cs	4 x10^{-4}	d^{-1},	Kirchner & Daillant (2002)
	Lichen, Sr	4 x10^{-4}	d^{-1},	Kirchner & Daillant (2002)

Table B.2. Concentration ratios (CRs, activity concentration in whole organism divided by activity concentration in soil) for terrestrial ecosystem from IAEA (2014) – arithmetic mean values.

Element	Organism	CR (Bq kg^{-1} f.w. per Bq kg^{-1} d.w)
Cs	Wildgrass/grasses	1.8
Sr	Wildgrass/grasses	1.8
Cs	Shrubs	2.3
Sr	Shrubs	0.5
Cs	Lichen	4.1
Sr	Lichen	4.8

Although some information exists on soil to grass transfer for the short term after accidents (Fesenko et al., 2009) these data are, by the author's own admission, insufficient for adequate (CR) estimation. This, coupled to the knowledge that, with the model constructed and parameterized in its current configuration, direct contamination by fallout dominates the total activity concentration in vegetation in the initial weeks of simulation renders the application of highly uncertain CR values relatively unimportant.

Contaminated lichens may be an important source of radiocaesium to reindeer during summer (Staaland et al., 1995). For this reason, the CR data for this biota category is also included in Table B.2. and for subsequent modelling calculations. It is important to note that output data for shrubs have been used as input to the assessment of ingestion doses for humans by assuming that shrub contamination levels provide a reasonable proxy for edible berries.

Finally, translocation is often accounted for in assessments with agricultural systems. Translocation is the process leading to the redistribution of a chemical substance deposited on the aerial parts of a plant to other parts that have not been contaminated directly (IAEA, 2010). Since the hypothetical accident has been assumed to coincide with the time of year when berries might be harvested the requirement to account for this process was not obvious and was therefore not attempted.

For mammals, examples of (bio)kinetic model for terrestrial environments have been published in the open literature and one of these, the so-called FASTer model, has been selected for further application (Brown et al., 2003; Beresford et al., 2010). For herbivorous mammals, the input data used can be those specifying the activity concentrations in grass as expressed above. Details are required regarding biokinetic parameters for various representative animals/fauna as described below.

required regarding biokinetic parameters for various representative animals/fauna as described below.

$$\frac{dC_{r,a}}{dt} = \sum_{i=1}^{i=n}\left(x_i . AE_{r,i} . {FMI}/_{M} . C_{r,i}\right) - C_{r,a} . \lambda_{r,a} \qquad \text{(B-3)}$$

Where :

x_i is the fraction of the diet associated with dietary component ''i'';

$AE_{r,i}$ is the assimilation efficiency(dimensionless) for radionuclide "r" within dietary component "i";

FMI/M is the ingestion rate per unit mass of animal (kg f.w. day^{-1} per kg f.w.);

$C_{r,i}$ is the activity concentration of radionuclide "r" in dietary component ''i'' (Bq kg^{-1} f.w.);

$C_{r,a}$ is the ''whole-body'' activity concentration of radionuclide "r" in the animal (Bq kg^{-1} f.w.); and

$\lambda_{r,a}$ is the effective loss rate of radionuclide "r" from animal (day^{-1}) incorporating both excretion rate and physical decay of the radionuclide.

This model has been applied to determine the transfer to deer/herbivorous mammal and rat/burrowing mammal.

A special note should be made of the use of output data from the FASTer model. As the activity concentrations predicted pertain to the whole body of deer and game animals some account needs to be taken of the consideration that people are not eating the entire animal, for example bone should be excluded. For this reason, an additional factor was considered to account for the fraction of total body activity that is in the soft tissues of herbivores (relative units). A value of 1 for Cs and 0.1 for Sr was used in line with the assumption made in Beresford et al. (2008b).

Fresh matter ingestion rates, FMI have been derived using allometric relationships of the form given in equation (B-4) as shown in Table B.3. The masses for Rat/burrowing mammal have been extracted from ICRP (2008). Since for Deer/herbivorous mammal, the obvious candidate for analyses would be Reindeer (*Rangifer tarandus*), it is possible to be more specific with the appropriate masses to be used. Although selecting a representative mass for an adult of a particular species is not uncontentious, because of uncertainties associated with seasonal changes and differences between the sexes, a value of 100 kg, based on a cursory synthesis of the data collated by Finstad & Prichard (2000), might not be considered entirely groundless. The following allometric relationship can thus be applied:

$$FMI = a.M^{b} \qquad \text{(B-4}$$

where

a is the multiplication constant in the allometric relationship for fresh matter intake for animal [kg d^{-1}] b is the exponent in the allometric relationship for fresh matter intake for animal [relative units] M is mass of the animal (kg)

Table B.3. Fresh matter ingestion rates, FMI, for the various animals selected for study

Organism	FMI (kg/d)	Comments and references
Deer/herbivorous mammal	3.6E+00	Mass = 100 kg (Finstad. & Prichard (2000)); FMI for herbivores (kg d^{-1}) = $0.1995M^{0.628}$ from Nagy (2001)
Rat/burrowing mammal	8.4E-02	Mass = 0.314 kg (ICRP, 2008); FMI for Rodentia (kg d^{-1}) = $0.2296M^{0.864}$ from Nagy (2001)

Similarly, $\lambda_{r,a}$ the effective loss rate of radionuclide "r" from animal, a, can be derived using allometric relationships (Table B.4).along with the animal masses specified above (Table B.3). The various parameters required in the model runs are thus specified in Table B.5.

Table B.4. Allometric equations used to derive effective loss rates (d^{-1}) for studied animals from mass of animals (kg) (Brown et al., 2003).

Radionuclide	*Allometric equ.s*
Cs	$\lambda_{r,a} = \frac{ln\,2}{18.36M^{0.24}}$
Sr	$\lambda_{r,a} = \frac{ln\,2}{645W^{0.26}}$

Table B.5. Parameters used in dynamic model runs.

Parameter	Dependencies : fauna, flora,radionuclide	Value	Units	Notes (references)
x_i	Grass (Deer)	0.75	dimensionless	Åhman (2007)
	Lichen (Deer)	0.25	dimensionless	
AE	Deer, Cs	1	dimensionless	USDoE (2002);
	Deer, Sr	0.3	dimensionless	USDoE(2002), ICRP 1979 (Part 1)
FMI/M	Deer	3.6E-02	kg f.w. day^{-1} per kg	(FMI/M)
	Rat	2.7E-01	kg f.w. day^{-1} per kg	(FMI/M)
$\lambda_{r,a}$	Deer, Cs	1.3E-02	d^{-1}	Table B.4; Mass = 100 kg
	Deer, Sr	3.2E-04	d^{-1}	Table B.4; Mass = 100 kg
	Rat, Cs	5.0E-02	d^{-1}	Table B.4; Mass = 0.314 kg
	Rat, Sr	1.5E-03	d^{-1}	Table B.4; Mass = 0.314 kg

The fraction dietary intake of lichen, grass and other vegetation in the diet of reindeer for the period in question is of course unknown but an assumption of 75 % grass intake by mass for September, as adopted by Åhman (2007), and assuming the rest of the diet comprises of lichen can be considered a reasonable first estimate. The inclusion of lichen in the summer diet will have the tendency to yield a conservative estimate of transfer to reindeer.

6.3 Appendix C – Modelling doses to humans and the environment

Once activity concentrations are derived, models are required to derive dose estimates for both a representative person and representative plants and animals. Standard methodologies were used for the calculation of human exposures (see e.g. IAEA, 2003) from various exposure pathways. The pathways of exposure considered were:

- Ingestion from contaminated foodstuffs
- Inhalation of radionuclides
- Exposure arising from a passing plume of contamination - cloud-shine
- Exposure from contaminated soil or shore sediments

The total annual effective dose from the ingestion of food, $E_{ing,\ food,\ public}$ (in Sv/a), has been calculated using equation:

The total annual effective dose from the ingestion of food, $E_{ing,\ food,\ public}$ (in Sv/a), has been calculated using equation:

$$E_{ing,food,public} = \sum_k H_B(k) \sum_j \left[C_B(j,k) DC_{ing,j}(j)\right] \quad \text{(C-1)}$$

where:

$H_B(k)$ is the rate of human consumption of foodstuff k (in kg/a);
$DC_{ing}(j)$ is the dose coefficient for ingestion of radionuclide j (in Sv/Bq); these values will be taken from ICRP publication (ICRP, 1995a)

$C_B(j,k)$ is the concentration of radionuclide j in the edible fraction of foodstuff k (in Bq/kg, fresh weight)

The activity concentrations in foodstuffs (for either marine or terrestrial products) were obtained via the kinetic models described in Appendix A and B.

The (annual) effective dose (Sv) to an individual from inhalation of radionuclides from a passing plume, $E_{inh,pers}$ (in Sv/a), has been calculated using the equation:

$$E_{inh,pers} = \sum \left[C_{a,time-\mathrm{int}}(j)\, DF_a(j)\, BR_{pers} \right] \quad \text{(C-2)}$$

where:

$DF_a(j)$ is the dose coefficient for inhalation of radionuclide j (in Sv per Bq); from ICRP (1995b)
$C_{a,\ time\text{-}int}(j)$ is the time integrated air concentration of radionuclide j in air (in Bq h/m^3).

The exposure arising from cloud-shine has been derived as follows:

$$E_{cs,pers} = \sum \left[C_{a,time-\mathrm{int}}(j)\, DF_{a,cs}(j) \right] \quad \text{(C-3)}$$

where:

$DF_{a,cs}(j)$ is the dose coefficient for cloud shine : (Sv h^{-1} Bq^{-1} m^3);

$C_{a,\ time\text{-}int}(j)$ is the time integrated air concentration of radionuclide j in air (in Bq h/m^3).

Finally, the annual effective dose to people from external exposure to radionuclides deposited on soil or sediment/shore line, $E_{ext,\ public}$ (in Sv/a), can be calculated using the equation

$$E_{ext,pers} = t_{pers} \sum \left[C_s(j)\, DF_{gr}(j) \right] \quad \text{(C-4)}$$

where:

t_{pers} is the time spent by person in contact with the contaminated soil/shore-sediment in a year (in h);
$DF_{gr}(j)$ is the dose coefficient for ground contamination of radionuclide j (in Sv/h per Bq m^{-2});
$C_S(j)$ is the surface contamination of radionuclide j in the shore sediments (in Bq m^{-2}).

6.4 Appendix D – Environmental risk assessment

The methodology that was used in parallel for terrestrial and aquatic ecosystems was based around the ERICA Integrated Approach (Larsson, 2008).The approach was designed to provide guidance on impacts of radioactivity on the environment to ensure that decisions on environmental issues give appropriate weight to the exposure, effects and risks from ionising radiation. Emphasis was placed on protecting the structure and function of ecosystems from radionuclides (Larsson, 2008), and supporting software (the ERICA Tool) was developed to serve this purpose (Brown et al., 2008).

Once activity concentrations in environmental media and biota have been collated and calculated, dose-rates will be derived through application of the ERICA Tool.

The basic underlying equations (Equations D-1 and D-2) utilise activity concentration data in order to derive internal (Dint) and external (Dext) absorbed dose-rates (in units of μGy h^{-1}). The total absorbed dose-rate is the sum of these components, through the application of dose conversion coefficients (DCCs).

$$\dot{D}^{b}_{int} = \sum_{i} C^{b}_{i} * DCC^{b}_{int,i} \quad \text{(D-1)}$$

where:

C_i^b is the average concentration of radionuclide *i* in the reference organism *b* (Bq kg^{-1} fresh weight),

$DCC_{int,i}^b$ is the radionuclide-specific dose conversion coefficient (DCC) for internal exposure defined as the ratio between the average activity concentration of radionuclide *i* in the organism *j* and the dose rate to the organism b (μGy h^{-1} per Bq kg^{-1} fresh weight).

$$\dot{D}_{ext}^b = \sum_z v_z \sum_i C_{zi}^{ref} * DCC_{ext,zi}^b \quad \text{(D-2)}$$

where:

v_z is the occupancy factor, i.e. fraction of the time that the organism *b* spends at a specified position *z* in its habitat.

C_{zi}^{ref} is the average concentration of radionuclide *i* in the reference media of a given location *z* (Bq kg^{-1} fresh weight or dry weight (soil or sediment) or Bq l^{-1} (water)),

$DCC^j_{ext,zi}$ is the dose conversion coefficient for external exposure defined as the ratio between the average activity concentration of radionuclide *i* in the reference media corresponding to the location *z* and the dose rate to organism *b* (μGy h^{-1} per Bq kg^{-1} fresh weight or Bq l^{-1}).

A further note is required in relation to calculation of dose-rates for benthic organisms, i.e. molluscs and crustaceans. In these particular cases a conversion is required between the radionuclide activity concentration in water and those in sediments since these organisms will receive a substantial component of dose from the seabed. The conversion has been made by using a distribution coefficient, k_d, taken from the default values provided in the ERICA Tool (Brown et al., 2016c). Molluscs and crustaceans are assumed to be permanently at the sediment-water interface thus receiving 50 % of their dose from the overlying water column and 50 % from underlying sediments.

The DCCs used correspond to those reported in ICRP (2008). Occupancy factors for organisms have been selected such that they might characterise a simplified yet realistic exposure geometry (Table D.1.).

Table D.1. Summarised source target exposure geometry for selected organisms

Organism	Exposure geometry assumption
Rat/burrowing mammal	In soil, volumetric source
Deer/herbivorous mammal	On soil, volumetric source

The dosimetric calculation underpinning the derivation of DCCs is dealt with in detail elsewhere (Ulanovsky and Pröhl, 2006; Ulavnovsky et al., 2008). Radioactive progeny are included in the DCCs of their parent if their half-lives are shorter than 10 days. DCCs for internal exposure were derived assuming a homogeneous distribution of the radionuclide in the organism; the error introduced by this assumption is, in view of the assessment goals, considered to be of minor significance (Gómez-Ros et al., 2008).

ISSN 2535-7379

dsa@dsa.no
+47 67 16 25 00
dsa.no

1 DSA Report 01-2021
DSA Regulatory Support to Kazakhstan, Kyrgyzstan and Tajikistan, 2017–2020

2 DSA-rapport 02-2021
Luftovervåkningsrapport 2020

3 DSA Report 03-2021
Risk and safety assessments supporting regulatory supervision of decommissioning and waste management for nuclear research and radiation facilities.

4 DSA Report 04-2021
Environmental impact assessment for activities during preparation and retrieval of spent nuclear fuel from dry storage unit 3A at Andreeva Bay

5 DSA Report 05-2021
Environmental Impact Assessment of a hypothetical accident during ship transport of spent nuclear fuel from Andreeva Bay

DSA
Norwegian Radiation and Nuclear Safety Authority